

# Interface and mixing zone between soil waters arising from upward and downward seepage - Part I: Homogeneous total density

D. van de Craats<sup>a,b,\*</sup>, C.J. van Duijn<sup>c</sup>, P.A.C. Raats<sup>d</sup>

<sup>a</sup> Soil Physics and Land Management, Wageningen University, Wageningen, The Netherlands

<sup>b</sup> Soil, Water, Land Use, Wageningen Research, Wageningen, The Netherlands

<sup>c</sup> Department of Mechanical Engineering, Eindhoven University of Technology, Eindhoven, The Netherlands

<sup>d</sup> Wageningen University and Research (WUR), Wageningen, The Netherlands

## ARTICLE INFO

### Keywords:

Rain water lens  
Mixing zone  
Solute transport  
Drainage  
Oscillatory flow  
Sharp interface

## ABSTRACT

Thin water lenses floating on top of the main groundwater body are important for many natural and agricultural systems, owing to their different properties in terms of chemical composition or density compared to the surrounding groundwater. In settings with upward seeping groundwater, lenses may form that have thicknesses ranging from tens of centimeters to a few meters, making them prone to changing conditions in the short (seasonal) or long term (climate change). Knowing their thickness, shape, movement and mixing zone width may help in managing these lenses.

In a series of two papers, we present a mathematical description of the flow of water and transport of solute in a 2D cross-section between two parallel outflow faces and compare a simplified model to a complete model as described by the numerical code SUTRA. In this first paper of the series, we consider situations with a homogeneous density distribution. In the simplified model we employ the sharp interface approximation to obtain an expression for the stream function, the interface between the two types of water and the corresponding maximum lens thickness in steady state in the domain considered. This steady state description is used for travel time analyses and forms the basis for the transient analyses. For a typical example of oscillatory (e.g. seasonal) fluctuations in boundary conditions, we obtain expressions of the movement of the interface midway between two outflow faces by separating the problem into two timescales using the interface motion equation. This analysis provides insight into the importance of parameters on the vulnerability of water lenses under changing conditions, and may easily be extended to situations with abrupt or gradual changes in boundary conditions reflecting changes in land use or climate, respectively. Finally, we derive an analytical approximation of the mixing zone midway between the drains for steady state solutions, stepping away from the sharp interface approach. For a variety of examples, we validate the obtained expressions of the simplified mathematical model against the numerical model code SUTRA, which solves the fluid and solute mass balances explicitly.

## 1. General introduction

The presence of shallow (fresh) water lenses is of importance in many natural and manmade groundwater-dependent (eco)systems. Shallow water lenses can be found in locations as fen meadows, floating fens, shallow coastal or river dunes and creek ridges (e.g. Cirkel et al., 2014; Schot et al., 2004; Stofberg et al., 2016; Wassen and Joosten, 1996), but also in agricultural areas in coastal zones with saline groundwater (e.g. Carol et al., 2018; de Louw et al., 2011; de Louw et al., 2013, Marconi et al., 2011; Velstra et al., 2011). Often these systems are influenced by human activity, either as side effect of e.g. enhanced drainage (e.g.

Delsman et al., 2017; Stofberg et al., 2017) or irrigation (Vandenbohede et al., 2014) or deliberately to increase fresh water availability (Pauw et al., 2015).

The shallow water lenses considered here, form when upward seepage of groundwater and downward infiltration of recharge water occur simultaneously for at least part of the year. The lenses are situated between outflow faces, parallel drains or ditches in the context of this paper, through which excess water is discharged, and have a typical thickness of tens of centimeters to a few meters, as opposed to fully-developed thick freshwater bodies in e.g. coastal dunes where the influence of upward seepage is negligible (Badon-Ghijben, 1888;

\* Corresponding author.

E-mail address: [daniel.vandecraats@wur.nl](mailto:daniel.vandecraats@wur.nl) (D. van de Craats).

<https://doi.org/10.1016/j.advwatres.2024.104793>

Received 9 February 2024; Received in revised form 4 June 2024; Accepted 17 August 2024

Available online 19 August 2024

0309-1708/© 2024 The Author(s). Published by Elsevier Ltd. This is an open access article under the CC BY license (<http://creativecommons.org/licenses/by/4.0/>).

Herzberg, 1901).

Two aspects of the soil aqueous solution may be of importance with respect to water lenses: its chemical composition, and the spatial distribution of its density. The chemical composition of the soil solution is an important factor in relation to plant growth, thus affecting the suitability of the soil for agriculture and horticulture (Pauw, 2015), and determining, together with other growth factors, the type of natural vegetation that might establish itself (Herbert et al., 2015; Schot et al., 2004). For agriculture, the most relevant factor in situations with saline groundwater may be the availability of sufficient fresh water in a relatively thick water lens, whereas for natural situations with fresh groundwater, a limited lens thickness may be preferred, providing gradients in water quality within plant root zones sustaining a high biodiversity (Bedford and Godwin, 2003). The chemical composition depends on the source of the water (Cirkel et al., 2014), in the context of this paper infiltrating precipitation or irrigation water and upwelling groundwater at the specific location. The spatial distribution of the density is an important factor in the dynamics of the soil aqueous solution (e.g. Werner et al., 2013), which plays an important role in salt affected coastal lowlands.

The thickness and volume of the rainwater lens can be measured or modelled for the purpose of, e.g., restoration of natural habitats, optimization of fresh water use in agriculture, or scenario analyses of climate change and sea level rise (Pauw, 2015; Stofberg et al., 2017). To do so, the interface between the two types of water should be determined. This interface may be approximated as a sharp interface by excluding any mixing processes, as is seen regularly in the literature (Werner et al., 2013). Although the sharp interface approximation allows relatively simple analytical methods, measurements (e.g., De Louw et al., 2011, De Louw et al., 2013) and numerical models (e.g., Eeman et al., 2011) show that the transition between the two water types is not sharp, but gradual as a result of molecular diffusion and dispersion (Eeman et al., 2011). We refer to this gradual transition as the mixing zone. De Louw et al. (2013) defined the center of the mixing zone as the point where the salinity is half that of the salinity of upward seeping water. They measured that for a drained agricultural field, this point moves through the soil very gradually, with variations on a seasonal timescale. This as opposed to the total water lens thickness, that has a more variable distribution due to day to day variations in (shallow) groundwater levels.

Most of the current work regarding shallow water lenses, its mixing zone and transient behaviour relies on the use of computationally intensive and knowledge demanding numerical models, such as the models SUTRA (Eeman et al., 2011; Voss and Provost, 2002), MODFLOW (Cozzolino et al., 2017), SEAWAT (De Louw et al., 2013) or MOCDENS3D (De Louw et al., 2011). This clearly adds in the understanding of processes for specific conditions. However, analytical formulations do provide a more fundamental understanding of the processes involved in the formation and development of these shallow water lenses. They also allow for fast calculations of lens characteristics for a broad range of parameter values, simplifying analyses as performed in Eeman et al. (2012) and Pauw et al. (2015) with numerical model results.

To date, only a limited number of analytical solutions is available where both the main groundwater body and the lens water are moving (Werner et al., 2013), with most solutions considering a steady state with a sharp interface approximation and without mixing and density effects. For equally spaced parallel drains, a steady state solution of the interface position under the assumption of a sharp interface without density effects is found in Poot and Schot (2000), albeit without any derivation. Maas (2007) provides a solution for a steady and transient situation, considering a sharp interface, movement of both types of water and also density effects, but he considers an oceanic island rather than the terrestrial, smaller scale situation of interest in this contribution. Despite this important difference in boundary conditions, several authors (Delsman et al., 2017; Eeman et al., 2011; Stofberg et al., 2017)

concerned with (modelling) rainwater lenses between parallel drains or ditches, use the analytical result of Maas (2007) as if it applies to their situation. This clearly demonstrates the need for an analytical description fitting to this situation.

Very few analytical solutions are available on mixing zone characteristics based on two dimensional flow problems (Werner et al., 2013). An attempt was made (Eeman et al., 2012; Stofberg et al., 2017) to characterize mixing zone development for oscillating conditions in two dimensions based on analyses of Cirkel et al. (2015) for a one dimensional situation, but to our knowledge an estimate of the mixing zone thickness in steady state based on a two dimensional analysis is not available. The mixing zone is, however, highly relevant for the purpose of determining the exposure of roots at different depths to e.g. mineral-rich or brackish groundwater, as the mixing zone may extend well beyond the sharp interface.

In a pair of two papers, we therefore present a set of (semi-)analytical solutions to obtain the position of the interface between infiltrating recharge water and upward seeping groundwater, both without density effects in this Part I, and with density effects in the accompanying Part II (van de Craats et al., 2024). In both Parts I and II, analytical and numerical solutions with SUTRA (Voss and Provost, 2002) will be used side by side.

In this Part I, we determine for a system of parallel, equally spaced drain tubes the location of the interface, not only for steady state, but also for certain transient cases for which the interface between the two types of water is time dependent. Although we mainly use a sharp interface approach, in this Part I we also provide an analytical estimate of the mixing zone midway between the drains in steady conditions.

In Part II, we will deal with some aspects of the dynamical effects of density gradients. Classical examples of the latter include the combination of saline and fresh water in coastal dunes, where density differences are important in the formation of rainwater lenses on top of the intruding seawater (Badon-Ghijben, 1888; Herzberg, 1901). However, here we focus on the shallow water lenses in areas with upward seepage.

We dedicate these papers to the late Sjoerd van der Zee (1955-2022), to honour him for his excellent contributions in the realms of soil, surface-water, and groundwater pollution, and ecohydrology. Sjoerd studied soil physics and physical chemistry at Wageningen University with Gerard Bolt. Following that, he started his research career at the LGM (= Delft Soil Mechanics Laboratory) (1981-1984; for results see van Duijn and van der Zee, 1986). That introduced him to the opportunities of mathematical analysis, which inspired him in all his later work. His entire further career he was with Wageningen University. His 1988 PhD thesis on 'Transport of reactive contaminants in heterogeneous soil systems' (van der Zee, 1988), provided a rational basis for dealing with contamination of soils, surface water, and groundwater with phosphate, cadmium, and copper. Such applications dominated his research in the following 20 years. In a fundamental yet practical manner, he dealt with the important role of field variability.

In 2005, Sjoerd became Professor of Ecohydrology, with emphasis on physical, but also including chemical and biological aspects. Applications included transport of pharmaceutical products, plant protection substances, and pathogens. In recent years, the focal subject was salinity in semi-arid and coastal-humid environments, with novel attention for the interplay of periodicity and long-term trends. The subject of the present papers still had his full interest in the final months of his life, when he actively participated in our regular Teams Meetings.

### 1.1. Introduction to Part 1: Homogeneous total density

In this Part I we focus on situations with a homogeneous total density: a constant fluid density throughout the domain. We aim to provide a thorough description of the flow problem at hand, and therefore we first describe the most general problem setting of a 2D flow problem between two parallel drains (section 2), with simultaneously occurring upward seepage and downward recharge, and a discharging drain. This

setting includes also the unsaturated zone and presence and mixing of solutes as is used in the numerical modelling for Parts I and II (SUTRA; Voss and Provost, 2002) and represents the current practice to model such systems numerically. We then have to constrain this general setting to allow for an analytical solution to the flow problem at hand (section 3). For this, we first consider only flow of water without any mixing, i.e. a sharp interface between the two flow regimes. Also, we consider only saturated flow, no head build-up between parallel drains, which, consequently, means no seepage face at surface level, and we employ the Boussinesq approximation. Next, we derive the stream function and interface position as function of distance to the drain in a steady state and consider a practical application regarding travel time and – depth analyses (section 4).

In section 5, we extend the analysis to transient conditions to find an analytical solution to the interface movement midway between the drains following oscillating boundary conditions representing seasonal fluctuations in recharge and seepage. The solution is based on a two-scale expansion which was found to correspond very well to numerical results of the general flow problem. Again, we show a practical application, in which we consider the fluctuation in concentration in the drainage water. Finally, in section 6 we also consider the mixing zone midway between two drains, and find an analytical approximation of the solute concentration as function of depth, matching reasonably well with numerical model results. Understanding these gradients and the factors influencing them is relevant for ecohydrological predictions. Overall, the analytical results give an excellent understanding of the general behaviour of shallow water lenses from a sound theoretical background, and provide ways to quickly assess potential effects of changes to the drivers of the shallow lenses. Sections 4, 5 and 6 all provide relevant insights into practical, real-world situations, both for agricultural and natural systems.

## 2. Problem setting

In this section the physical-mathematical model for describing flow of water and transport of solutes in saturated and unsaturated soil is introduced. In both Part I and Part II, the numerical finite element model SUTRA version 2.2 (Voss and Provost, 2002) is used to solve those equations.

The fluid mass balance is given in its basic form as

$$\frac{\partial}{\partial t}(\eta S \rho) + \text{div}(\rho \vec{q}) = 0, \quad (1)$$

where  $\eta$  [-] is porosity,  $S$  [-] is water filled pore space ( $S = 1$  for saturated conditions,  $0 < S < 1$  for unsaturated conditions),  $\rho$  [ML<sup>-3</sup>] is fluid density including dissolved solute. Further,  $\vec{q} = (q_x, q_y)$  [LT<sup>-1</sup>] is the fluid discharge, given by Darcy's law

$$\vec{q} = -\frac{\kappa \kappa_r}{\mu} \left( \nabla p + \rho \vec{g} \vec{e}_y \right), \quad (2)$$

where  $p$  [ML<sup>-1</sup>T<sup>-2</sup>] is fluid pressure,  $\vec{g}$  [LT<sup>-2</sup>] the gravitational acceleration,  $\vec{e}_y$  the directional vector (0, 1),  $\mu$  [ML<sup>-1</sup>T<sup>-1</sup>] the fluid viscosity (assumed to be constant),  $\kappa$  [L<sup>2</sup>] the permeability tensor, which for a homogeneous, isotropic soil may be replaced by  $\kappa = \kappa I$ ,  $I$  [-] being the identity matrix, and  $\kappa_r$  [-] is the relative permeability ( $\kappa_r = 1$  for saturated conditions,  $0 < \kappa_r < 1$  for unsaturated conditions). In SUTRA, the Mualem-van Genuchten expressions are used for the relations  $S = S(p)$  and  $\kappa_r = \kappa_r(S)$  (Voss and Provost, 2002).

The mass balance for the solute reads

$$\frac{\partial}{\partial t}(\eta S \rho w) + \text{div}(\rho w \vec{q} - \eta S \rho D \nabla w), \quad (3)$$

where  $w$  [MM<sup>-1</sup>] is the mass fraction of solute given as mass solute per mass of total fluid. The fluid density is given as a linear function of the mass fraction of solute

$$\rho = \rho_0(1 + \beta w), \quad (4)$$

where  $\beta$  [-] is the salt expansion coefficient given by  $\beta = \frac{\partial \rho}{\partial w} \frac{1}{\rho_0}$  and where

$\rho_0$  [ML<sup>-3</sup>] is the density of pure water. The coefficient  $D$  in (3) models the effect of molecular diffusion and dispersion. It is given as

$$D = D_{mol} I + D_{disp}, \quad (5)$$

where  $D_{mol}$  [L<sup>2</sup>T<sup>-1</sup>] is the molecular diffusion coefficient and  $D_{disp}$  [L<sup>2</sup>T<sup>-1</sup>] is the dispersion tensor. This tensor is given in two dimensions by

$$D = \begin{bmatrix} D_{xx} & D_{xy} \\ D_{yx} & D_{yy} \end{bmatrix} = \frac{1}{\eta S |\vec{q}|} \begin{bmatrix} (\alpha_L |q_x|^2 + \alpha_T |q_y|^2) & (\alpha_L - \alpha_T) (|q_x| |q_y|) \\ (\alpha_L - \alpha_T) (|q_x| |q_y|) & (\alpha_T |q_x|^2 + \alpha_L |q_y|^2) \end{bmatrix}, \quad (6)$$

where  $|\vec{q}| = \sqrt{q_x^2 + q_y^2}$  [LT<sup>-1</sup>] is the magnitude of the fluid discharge and  $|q_x|$  and  $|q_y|$  are the absolute values of the discharge components. Further,  $\alpha_L$  and  $\alpha_T$  [L] are the longitudinal and transversal dispersion lengths, respectively.

We consider a situation where a series of equally spaced drains (separated by a distance of  $2L$  [L], and positioned at depth  $D$  [L] below soil surface) are present in a homogeneous, isotropic soil. Let the domain  $\mathcal{D} \subset \mathbb{R}^2$  be described in  $x$  and  $y$ , where  $x$  denotes the horizontal direction perpendicular to the drain and  $y$  denotes the vertical direction, positive when pointing upwards (A). We assume no flow occurs in the third dimension (i.e. parallel to the drains). Choosing the coordinates such that a drain is located at  $\{x = L, y = 0\}$ , vertical water divides exist at  $x = 0$  and  $x = L$  due to symmetry of this flow problem.

The domain in the numerical model SUTRA is given by (see also Fig. 1A)

$$\mathcal{D}_{num} = \{(x, y) : 0 < x < L, -H < y < D\}, \quad (7)$$

where  $H$  [L] is the numerical model depth, chosen sufficiently far down from the interface and mixing zone to avoid a direct influence on their positions. In  $\mathcal{D}_{num}$ , the unsaturated domain is considered in order to represent a real-world situation as closely as possible. This means that non-vertical flow through the capillary fringe, head buildup midway between the drains and a potential delay in flow due to the unsaturated zone are all accounted for.

In SUTRA, half a drain is modeled explicitly within the element mesh by excluding half a circle with a radius of 3 cm centered at  $\{x = L, y = 0\}$ , as in van de Craats et al. (2021). Mesh refinements are made in the proximity of the drain, to allow for multiple nodes on the drain circle.

Top and bottom boundary fluxes are given by uniform recharge ( $N$  [LT<sup>-1</sup>]) and seepage ( $K$  [LT<sup>-1</sup>]) fluxes, respectively, which are defined positive into the domain. Both recharge and seepage are required to have a net positive contribution for a water lens to form. In addition, the fact that they are defined as uniform fluxes does not allow the presence of a seepage face at the soil surface. Hence, groundwater levels must remain below the soil surface everywhere at all times.

Recharge and seepage are given a solute mass fraction of 0 and  $w_K$  [-], respectively, as given by

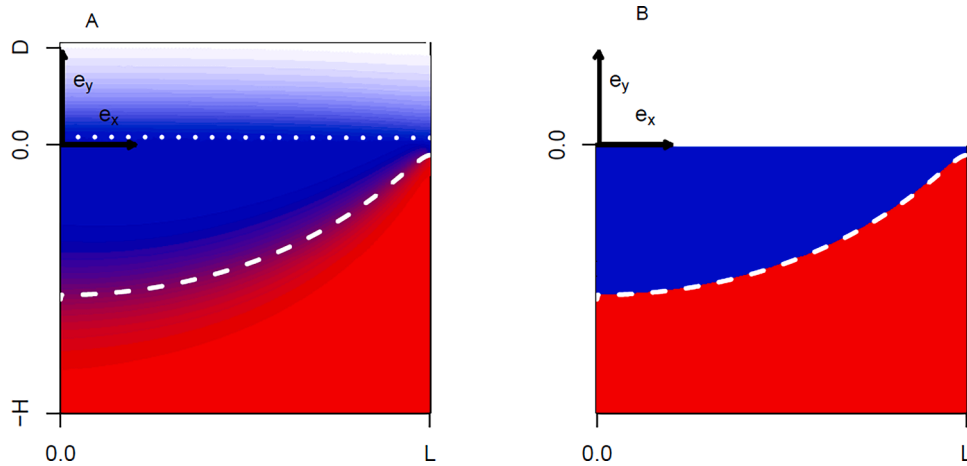


**Fig. 1.** (A) Schematic representation of a steady water lens as used in the numerical model, with the drain situated at  $(x,y)=(L,0)$  and vertical water divides at  $x = 0$  and  $x = L$ ,  $L$  denoting half of the drain distance. Upward seeping (red), and downward infiltrating (blue) water meet at the interface (dashed line), where mixing occurs as indicated by the gradual transition in colour. Above the groundwater table (dotted line) soil water content decreases gradually in the unsaturated zone (white shading). The maximum depth at  $-H$  is shifted upward for illustrative purposes. (B) Schematic representation used in the sharp interface approximation for the analytical model. No mixing occurs, and only the domain below the drain is considered, i.e. the partially saturated zone and head build-up midway between drains are disregarded. The bottom extends to minus infinity.

$$\begin{cases} w = w_N = 0, \vec{q} \cdot \vec{e}_y = -N \text{ along } 0 < x < L, y = D \\ w = w_K, \vec{q} \cdot \vec{e}_y = +K \text{ along } 0 < x < L, y = -H \\ \frac{\partial w}{\partial x} = \vec{q} \cdot \vec{e}_x = 0 \text{ along } x = 0, L \text{ and } y < D \end{cases} \quad (8)$$

Along the drain boundary with a radius of 3 cm, fixed pressure nodes are prescribed in SUTRA based on the nodes' vertical position, with a pressure ranging from 0 at the top node to  $587.4 \text{ kg m}^{-1} \text{ s}^{-2}$  at the bottom node, according to a hydrostatic equilibrium within the drain, assuming a fresh water density of  $998 \text{ kg m}^{-3}$  within the drain and a fully saturated drain with no excess pressure. Water and solute move out of the domain via fixed pressure nodes, following the local pressure gradients and solute mass fractions.

### 3. Simplified mathematical model setting

In this section we introduce a number of simplifying assumptions with respect to the physical problem and obtain a reduced setting that can be treated by (semi) analytical methods. In spite of the proposed simplifications, we show in sections 4-6 that in many cases of practical interest, the numerical (SUTRA) results and the constructed analytical expression are quite close.

The following additional assumptions are required:

1. The vertical domain changes to (Fig. 1B)

$$\mathcal{D} = \{(x,y) : 0 < x < L, -\infty < y < 0\}, \quad (9)$$

such that the drain is situated in the corner point  $\{x = L, y = 0\}$ .

2. The soil is fully saturated; i.e.  $S = 1$  everywhere in  $\mathcal{D}$ .
3. The Boussinesq approximation holds; i.e. in (1) - (3) we impose  $\rho = \rho_0$  (= constant), except in the gravity term of the Darcy equation (2).

Under these assumptions, the problem reduces to

$$\text{div}(\vec{q}) = \frac{\partial q_x}{\partial x} + \frac{\partial q_y}{\partial y} = 0, \quad (10)$$

$$\vec{q} = -\frac{\kappa}{\mu} \left( \nabla p + \rho g \vec{e}_y \right), \quad (11)$$

$$\frac{\partial w}{\partial t} + \text{div}(w \vec{q} - D \nabla w) = 0, \quad (12)$$

$$\rho = \rho_0(1 + \beta w), \quad (13)$$

in  $\mathcal{D}$  and for  $t > 0$ . The boundary conditions read:

$$\begin{cases} w = w_N = 0, \vec{q} \cdot \vec{e}_y = -N \text{ along } 0 < x < L, y = 0 \\ w = w_K, \vec{q} \cdot \vec{e}_y = +K \text{ along } 0 < x < L, y = -\infty \\ \frac{\partial w}{\partial x} = \vec{q} \cdot \vec{e}_x = 0 \text{ along } x = 0, L \text{ and } y < 0 \end{cases} \quad (14)$$

For the moment we leave the initial condition for the mass fraction unspecified.

The equations (10), (11) and (12) are coupled through the solute dependent density. For the flow field, we cross differentiate the components of Darcy's law (11), to obtain

$$\frac{\partial}{\partial y} \left( \frac{\mu}{\kappa} q_x \right) + \frac{\partial^2 p}{\partial x \partial y} = 0 \text{ and } \frac{\partial}{\partial x} \left( \frac{\mu}{\kappa} q_y \right) + \frac{\partial^2 p}{\partial x \partial y} + \frac{\partial}{\partial x} (\rho g) = 0, \quad (15)$$

which results in

$$\frac{\partial}{\partial x} \left( \frac{\mu}{\kappa} q_y \right) - \frac{\partial}{\partial y} \left( \frac{\mu}{\kappa} q_x \right) + \frac{\partial}{\partial x} (\rho g) = 0. \quad (16)$$

Eq. (10) is satisfied if we introduce the stream function  $\psi$  [ $\text{L}^2 \text{T}^{-1}$ ] according to

$$\vec{q} = (q_x, q_y) = \text{curl}(\psi) = \left( -\frac{\partial \psi}{\partial y}, \frac{\partial \psi}{\partial x} \right) = 0. \quad (17)$$

Substituting (17) into (16) yields for the stream function

$$\frac{\partial}{\partial x} \left( \frac{\mu}{\kappa} \frac{\partial \psi}{\partial x} \right) + \frac{\partial}{\partial y} \left( \frac{\mu}{\kappa} \frac{\partial \psi}{\partial y} \right) + \frac{\partial}{\partial x} (\rho g) = 0. \quad (18)$$

For a homogeneous soil and a fluid with constant viscosity, there results (De Josselin de Jong, 1960)

$$\nabla^2 \psi + \frac{\kappa}{\mu} \frac{\partial}{\partial x} (\rho g) = 0, \tag{19}$$

where  $\nabla^2$  denotes the Laplacian:  $\nabla^2 = \frac{\partial^2}{\partial x^2} + \frac{\partial^2}{\partial y^2}$ .

In Part I of this work we disregard the influence of spatial density variations on the flow. Hence  $\beta = 0$  and  $\rho = \rho_0$  in (13), implying that (10), (11) and (12) are decoupled, and (19) reduces to  $\nabla^2 \psi = 0$ . We treat three cases that are of practical interest in the remainder of this Part I. We define a reference situation which applies to all three cases, with parameter values given in Table 1.

#### 4. Steady state flow

##### 4.1. Mathematical model description

Let the recharge  $N$  and seepage  $K$  be given by positive constants to allow for the formation of water lenses between parallel drains. The boundary conditions (14) are satisfied if we choose for  $\psi$  along the boundary of  $\mathcal{S}$ :

$$\begin{cases} \psi(0, y) = 0 \text{ and } \psi(L, y) = KL \text{ for } y < 0 \\ \psi(x, 0) = -Nx \text{ and } \psi(x, -\infty) = Kx \text{ for } 0 < x < L \end{cases} \tag{20}$$

With these conditions, the strength of the drain is  $(N + K)L$  [ $L^2 T^{-1}$ ].

Though we do not consider actual solutes yet, we may separate our domain into two parts, which we refer to as the recharge part ( $\mathcal{S}_N$ ) and seepage part ( $\mathcal{S}_K$ ), respectively. In Fig. 1B, these are represented by the blue and red part, respectively. The recharge part consists of water entering through the top of the domain, the seepage part consists of water entering through the bottom of the domain. These domains are separated by a sharp interface  $I$  [L], which, in view of our boundary

**Table 1**

Parameter values used for the reference simulations in sections 4-6. For parameter values indicated with a \*, and parameters that are not mentioned in this table, we refer to Voss and Provost (2002) for a description and, if applicable, their standard value.

	Description	Parameter	SUTRA	Analytical	Unit
Dimensions	Half drain distance	$L$	5	5	m
	Drain depth	$D$	1.2	-	m
	Domain depth	$H$	8.8	-	m
Soil matrix properties	Porosity	$\eta$	0.45	0.45	$m^3$
	Residual water cont.*	$S_{res}$	0.149	-	$m^3$
	a-par MvG*	$\alpha$	2.0	-	$m^{-1}$
	n-par MvG*	$n$	1.41	-	-
	Permeability	$\kappa$	$8.772 \cdot 10^{14}$	$8.772 \cdot 10^{14}$	$m^2$
Fluid properties	Base density	$\rho_0$	998.0	998.0	$kg\ m^{-3}$
	Salt expansion coef.	$\beta$	0	0	-
	Viscosity	$\mu$	0.001	0.001	$kg\ m^{-1}\ s^{-1}$
Diffusion / Dispersion	Long. disp. length	$\alpha_L$	0.1	0.1	m
	Trans. disp. length	$\alpha_T$	0.01	-	m
	Molecular diff.	$D_m$	$1e^{-9}$	$1e^{-9}$	$m^2\ s^{-1}$
Boundary conditions	Recharge	$N$	0.0005	0.0005	$m\ d^{-1}$
	Seepage	$K$	0.0005	0.0005	$m\ d^{-1}$
	Solute mass fraction in $N$	$w_N$	0	0	$kg\ kg^{-1}$
	Solute mass fraction in $K$	$w_K$	0.03507	0.03507	$kg\ kg^{-1}$

conditions, is given in steady state as the streamline where  $\psi = 0$ , i.e.

$$\psi(x, y) = 0 \Leftrightarrow y = I(x) \text{ for } 0 < x \leq L. \tag{21}$$

The boundary conditions in terms of  $\psi$  (20) imply that  $\psi \leq 0$  across the boundary of  $\mathcal{S}_N$  and  $\psi \geq 0$  across the boundary of  $\mathcal{S}_K$ . Then, using the strong maximum principle (Alt and van Duijn, 1990), we have

$$\psi < 0 \text{ in } \mathcal{S}_N \text{ and } \psi > 0 \text{ in } \mathcal{S}_K. \tag{22}$$

The interface itself intercepts the drain and is assumed to be described by a continuous, increasing function of  $x$  between  $(0, L)$ , with  $I(L) = 0$ . Due to domain symmetry the interface is horizontal midway between the drains, implying

$$\frac{\partial I}{\partial x}(x=0) = 0. \tag{23}$$

In search of an explicit expression for the stream function in  $\mathcal{S}$ , we first remove the boundary conditions at  $x = 0, L$  and at  $y = -\infty$  by setting

$$u(x, y) = \frac{Kx - \psi(x, y)}{N + K}. \tag{24}$$

Clearly,

$$\nabla^2 u = 0 \text{ in } \mathcal{S},$$

and  $u$  satisfies the boundary conditions, see (20),

$$\begin{cases} u(0, y) = u(L, y) = 0 \text{ for } y < 0 \\ u(x, 0) = x \text{ and } u(x, -\infty) = 0 \text{ for } 0 < x < L \end{cases} \tag{25}$$

Given (21), the interface position  $I(x)$  can be described in terms of  $u$  as

$$u(x, y) = -\frac{Kx}{N + K} \Leftrightarrow y = I(x) \text{ for } 0 < x < L. \tag{26}$$

By separation of variables, we obtain the Fourier series solution for  $u$  as

$$u(x, y) = \sum_{n=1}^{\infty} \left( -\frac{2L}{n\pi} \cos(n\pi) \right) \sin\left(\frac{n\pi x}{L}\right) e^{\frac{n\pi y}{L}}. \tag{27}$$

With Mathematica (Wolfram Research, 2019), this expression can be resolved as

$$u(x, y) = \frac{2L}{\pi} \arctan \left( \frac{\sin\left(\frac{\pi x}{L}\right) e^{\left(\frac{\pi y}{L}\right)}}{1 + \cos\left(\frac{\pi x}{L}\right) e^{\left(\frac{\pi y}{L}\right)}} \right). \tag{28}$$

Using (24), the corresponding expression for the stream function in  $\mathcal{S}$  reads

$$\psi(x, y) = Kx - (N + K) \frac{2L}{\pi} \arctan \left( \frac{\sin\left(\frac{\pi x}{L}\right) e^{\left(\frac{\pi y}{L}\right)}}{1 + \cos\left(\frac{\pi x}{L}\right) e^{\left(\frac{\pi y}{L}\right)}} \right). \tag{29}$$

The horizontal and vertical water discharge components follow from (29) and (17) as

$$q_x(x, y) = -\frac{\partial \psi(x, y)}{\partial y} = (N + K) \frac{\sin\left(\frac{\pi x}{L}\right)}{\cos\left(\frac{\pi x}{L}\right) + \cosh\left(\frac{\pi y}{L}\right)}, \tag{30}$$

and

$$q_y(x, y) = +\frac{\partial \psi(x, y)}{\partial x} = -\left( N + (N + K) \frac{\sinh\left(\frac{\pi y}{L}\right)}{\cos\left(\frac{\pi x}{L}\right) + \cosh\left(\frac{\pi y}{L}\right)} \right). \tag{31}$$

Note that the horizontal discharge is zero for  $x = 0$  and  $x = L$ ,

satisfying the properties of a vertical water divide.

We are particularly interested in the interface between the two types of water. It is found by solving, see also (26),  $u(x, y = I(x)) - \frac{K}{N+K}x = 0$  for  $0 < x < L$ . Applying the Fourier expansion to both terms, we have

$$u(x, y = I(x)) = \sum_{n=1}^{\infty} \left( -\frac{2L}{n\pi} \cos(n\pi) \right) \sin\left(\frac{n\pi x}{L}\right) \left( e^{\left(\frac{n\pi I(x)}{L}\right)} - \frac{K}{N+K} \right) = 0, \quad (32)$$

for  $0 < x < L$ . Again, we use Mathematica (Wolfram Research, 2019) to resolve this expression. The result is

$$I(x) = \frac{L}{\pi} \ln \left( \frac{\sin\left(\frac{K}{N+K} \frac{\pi x}{2L}\right)}{\sin\left(\frac{2N+K}{N+K} \frac{\pi x}{2L}\right)} \right) \text{ for } 0 < x \leq L, \quad (33)$$

which is equivalent to the result in Poot and Schot (2000). A straightforward calculation shows that

$$\frac{dI}{dx}(x=L) = \tan\left(\frac{N}{N+K} \frac{\pi}{2}\right). \quad (34)$$

Note that (33) and (34) show that the flux ratio  $K/N$  drives the interface position. The maximum interface depth is reached midway between the drains at  $x = 0$ . From (33) we find

$$h := I(0) = \frac{L}{\pi} \ln\left(\frac{K}{2N+K}\right). \quad (35)$$

At  $x = 0$ , the vertical discharge is given by

$$\begin{aligned} q_y(0, y) &= - \left( N + (N+K) \frac{\sinh\left(\frac{\pi y}{L}\right)}{1 + \cosh\left(\frac{\pi y}{L}\right)} \right) \\ &= -N + K \left( \frac{N}{N+K} + \frac{e^{\left(\frac{\pi y}{L}\right)} - 1}{e^{\left(\frac{\pi y}{L}\right)} + 1} \right). \end{aligned} \quad (36)$$

Hence, with (35),

$$\begin{aligned} q_y(0, y) &= 0 \text{ at } y = h \\ q_y(0, y) &> (<) 0 \text{ if } y < (>) h. \end{aligned} \quad (37)$$

In order to compare analytical interfaces, determined with the sharp interface approach, with numerical model results of the fluid and solute mass balance, a definition of the interface is required for the numerical model. For this we use the (central) moments of the vertical solute mass fraction gradient, similar as in e.g. Eeman et al. (2011), where the first moment gives the vertical position of the interface with respect to the drain, and the second central moment provides a measure of the mixing zone width. To account for the curvature in the groundwater table, which in SUTRA is situated at  $p(x, y) = 0$ , lens thickness is obtained by subtracting the first moment from the groundwater table position.

An interesting application of the steady state problem is related to average residence times and travel time distributions, which are relevant for e.g. the available time for a constituent to break down in the groundwater, before exfiltrating into the drain. The average residence time of water in the lens ( $T_{res}$  [T]) is given as

$$T_{res} = \frac{\eta A_l}{NL} = \frac{\eta}{\pi N} \int_0^L \left( -\ln \left( \frac{\sin\left(\frac{K}{N+K} \frac{\pi x}{2L}\right)}{\sin\left(\frac{2N+K}{N+K} \frac{\pi x}{2L}\right)} \right) \right) dx, \quad (38)$$

where  $A_l$  [ $L^2$ ] is the area of the water lens in the half strip. It is obtained by integrating (33) from  $x = 0$  to  $x = L$ . This integral can, in principle, be evaluated. However, as the resulting expression is lengthy and not

straightforward to interpret, we do not show its evaluated form in (38). Not only the average residence time, but also the travel time from any position at the top of the groundwater table towards the drain may be of importance. The flow path of a water droplet entering the domain at  $r_{ent} = (x, y) = (x_{ent}, 0)$ , with  $0 < x_{ent} < L$ , and leaving the domain through the drain at  $r_{drm} = (x, y) = (L, 0)$  is given as the streamline with value  $\psi_{rent} = -Nx_{ent}$ . For any point  $(x, y)$  along this streamline the water flow velocity may be obtained from (30) and (31) and the porosity. The travel time  $T_{tr}$  [T] of a water particle is then obtained as

$$T_{tr} = \int_{\psi_{rent}}^{\psi_{drm}} \frac{\eta}{|q(r)|} ds = \int_{r_{ent}}^{r_{drm}} \frac{\eta}{\sqrt{q_x^2(r(t)) + q_y^2(r(t))}} |r'(t)| dt, \quad (39)$$

where  $r(t) = (x(t), y(t))$  is the parameterization of the streamline and the integration bounds  $r_{ent}$  and  $r_{drm}$  form the points of entrance and exit of the domain. This expression is evaluated numerically.

We can also obtain the maximum depth that a droplet, entering the domain at  $r_{ent}$ , reaches while traveling through the domain. For each depth  $y$  in  $h < y < 0$  there exists one streamline originating from  $(x, 0)$  with a horizontal tangent at that specific depth. For any such point, this means that a flux of  $-\psi(x, y)$  reaches to depths below  $y$ , whereas the remaining recharge  $(N + \psi(x, y))$  never reaches this depth. Denoting the coordinates of the deepest point of each streamline by  $(x_d, y_d)$ , we may find the horizontal position by considering  $q_y(x_d, y_d) = 0$ . With (31), we find for any vertical position in  $h < y_d < 0$  the corresponding horizontal position  $x_d$  as

$$x_d = \frac{L}{\pi} \arccos \left( -\frac{K+N}{N} \sin\left(\frac{\pi y_d}{L}\right) - \cosh\left(\frac{\pi y_d}{L}\right) \right). \quad (40)$$

The stream function value corresponding to the coordinates  $(x_d, y_d)$  can now be obtained from (29), which can directly be used to find the point of origin of the water droplet at  $(x_d, y_d)$ , as  $\psi_{rent} = -Nx_{ent}$ .

## 4.2. Example results

Steady state flow patterns for three situations are shown in Fig. 2, with the middle panel corresponding to the reference situation (Table 1), and the other panels deviating in flux ratio only. Recharge water infiltrates uniformly at the top of the domain and flows towards the drain situated in the top right corner at  $\left(\frac{x}{L}, \frac{y}{L}\right) = (1, 0)$ . Seepage water infiltrates at the bottom, flows in an upward direction and is then also diverted towards the drain. The streamline  $\psi = 0$  separates negative stream function values (in blue) from positive stream function values (in red). It can readily be seen that this streamline indeed divides the domain  $\mathcal{D}$  in a recharge part ( $\mathcal{S}_N$ ) and seepage part ( $\mathcal{S}_K$ ), such that it acts as the interface as defined in (21). The deepest part of the rainwater lens is found midway between the drains. Here, also the lowest flow velocities occur, with a stagnation point at the intersect between the vertical water divide and the interface. It follows directly from (33) and (35) that dividing both  $x$  and  $y$  by half the drain distance, the dimensionless lens thickness is a function of flux ratio only, as demonstrated in Fig. 2. The larger the flux ratio, the smaller the (dimensionless) lens thickness.

Agreement between the interface obtained with the analytical sharp interface approximation and the numerical flow and transport model SUTRA with regard to the interface position is very good (Fig. 2), especially away from the drain. A difference between the two methods can be observed close to the drain, for which we identified three causes. (i) For the numerical model results, we opted for the simple approach of obtaining the interface position in the vertical direction only, rather than obtaining the interface position perpendicular to the flow direction (as in Eeman et al., 2011). As the derivative of the interface with respect to  $x$  is largest close to the drain, the largest errors present themselves in this region. (ii) The definition of the numerical interface is not identical

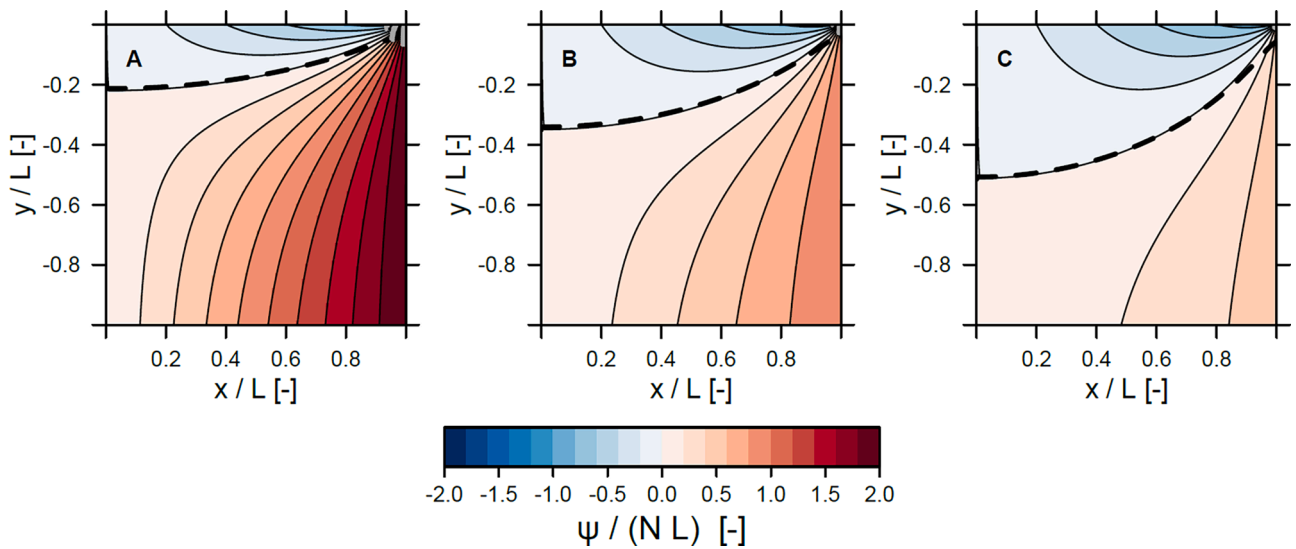


Fig. 2. Flow patterns obtained with (29) for flux ratios ( $K/N$ ) of 2, 1 and 0.5 in (A), (B) and (C), respectively, with (B) showing the reference situation (Table 1). Recharge rates are kept constant and seepage is varied between the panes. Black thin lines show stream lines, with the red shaded area indicating positive stream function values in the seepage part ( $\mathcal{S}_K$ ) and the blue shaded areas indicating negative values in the recharge water part ( $\mathcal{S}_N$ ), with the transition between the two being the interface. The dashed black line shows the interface obtained from SUTRA. The x- and y-axis are normalized by dividing by  $L$ .

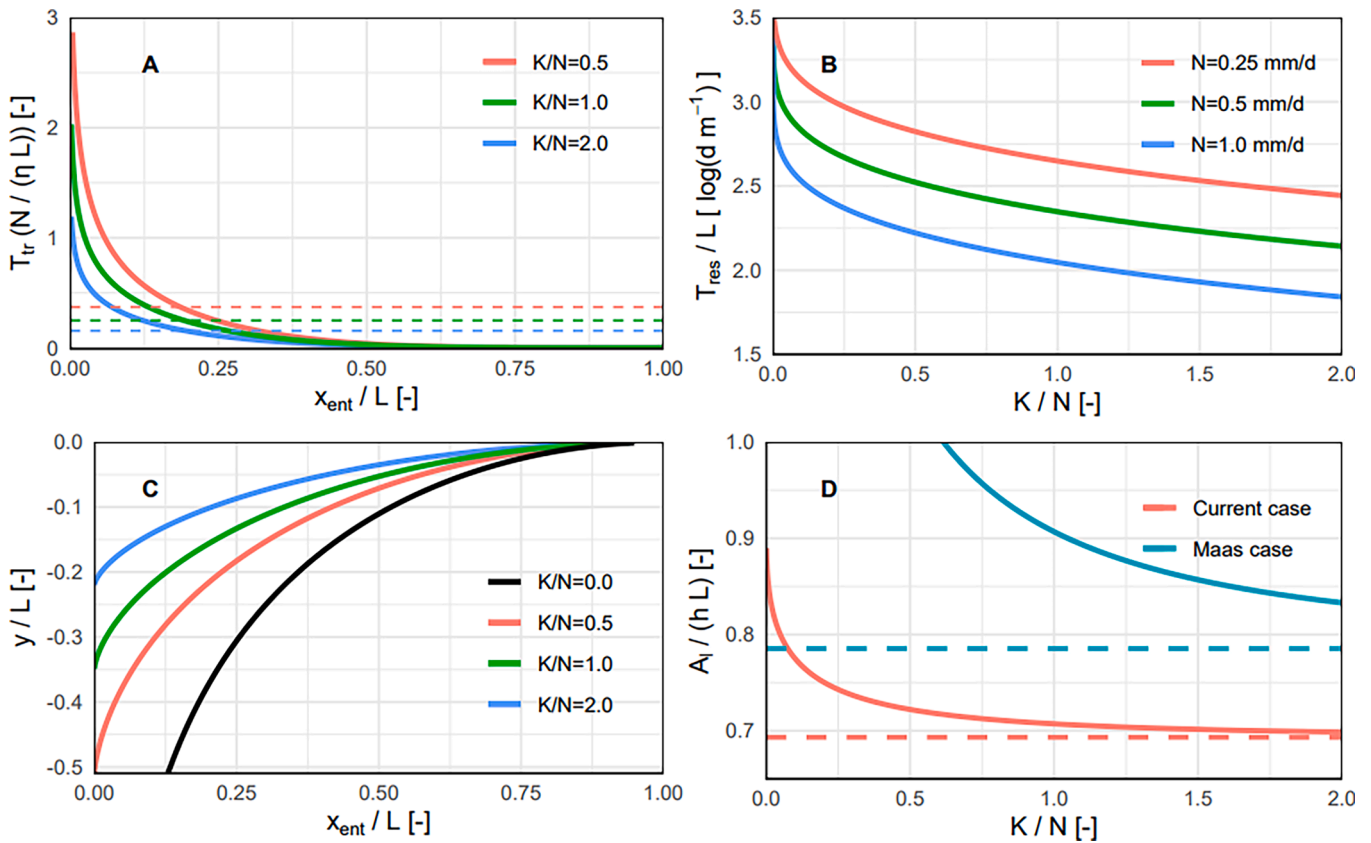


Fig. 3. (A) Travel time  $T_{tr}$  of a water droplet from point of origin ( $x_{ent}$ ) to the drain, as function of point of origin, for three flux ratios (indicated by color). Travel time and point of origin are both given in non-dimensional form as seen from the axis labels. The dotted horizontal lines indicate average residence times, obtained with (38). (B) Average residence times as function of flux ratio, for three recharge rates (indicated by color). Residence times (divided by half a drain distance  $L$ ) are given on log-scale on the y-axis. (C) Maximum travel depth of a water droplet as function of point of origin  $x_{ent}$ , for four flux ratios (indicated by color). Both axes are normalized by half a drain distance. (D) Ratio of lens area in the half strip over maximum lens thickness, divided by half the drain distance, as function of flux ratio. The horizontal dashed line shows the asymptote as  $A_l/h = \ln(2)$ . The case of Maas (2007) is shown for the purpose of comparison, with its horizontal asymptote given by  $A_l/h = \frac{\pi}{4}$ .

to the definition used in the analytical model. Especially in case of skewed distributions, using the first moment of the concentration gradient to describe the interface position may result in different results. In addition, (iii) the groundwater table in the numerical results does not intersect the drain, but may be situated somewhat above the drain, such that a pocket of water exists above the drain. As lens thickness in the analytical model is, per definition, zero at the drain, this results in a relatively large difference between the two methods close to the drain.

An example of the travel time of any water droplet entering between  $0 < x_{ent}/L < 1$  is given in Fig. 3A, for three flux ratios. The travel time itself was non-dimensionalized, such that this graph holds for any drain system configuration, recharge rate and porosity when properly scaled. Clearly, increasing the flux ratio results in decreasing non-dimensional travel times, as the water lens becomes thinner (35), which also immediately follows from the expression for the average residence times (38). This is demonstrated in Fig. 3B as well, showing the average residence time divided by half the drain distance, as function of flux ratio, for three different recharge rates. For a given flux ratio, an increase in recharge rate (and thus also seepage rate) results in a decrease in residence time, as water is required to move faster through the same lens area. Increasing flux ratios while maintaining the same recharge rate results in decreasing residence times due to shallower lenses.

Returning to Fig. 3A, for a flux ratio of 1, approximately 80% of the distance between  $0 < x < L$  discharges faster than the average residence time, which may have important implications for the breakdown or formation of certain constituents (e.g., in the process of denitrification in the anaerobic environment) while traveling through the saturated zone and thereby affect the composition of drainage water. This percentage increases even further for decreasing flux ratios. In the reference case, with  $K/N = 1$ ,  $N = 0.5 \text{ mm d}^{-1}$ ,  $\eta = 0.45$  and  $L = 5$ , the average residence time of a water droplet is approximately 1100 days. However, as much as 50% of the water infiltrating at the surface leaves the domain within 125 days, and 20% even within 4 days.

In Fig. 3C maximum travel depth of a particle entering the domain between  $0 < x_{ent}/L < 1$  is given (40), for four flux ratios, including a situation in which only recharge occurs (Groenendijk and van den Eertwegh, 2004). The maximum depth reached by a particle originating midway between two drains at  $x = 0$  is determined by (35), and reaches to minus infinity for the situation with  $K/N = 0$ . Again, we see that the majority of the water is discharged through a rather shallow layer, corresponding with the short travel times (Fig. 3A). Roughly 80% of the water is discharged through the layer between  $h/2 < y < 0$ , with the remainder of the water reaching to larger depths.

Dividing lens area  $A_l$  by maximum lens thickness,  $-h$ , and normalizing by drain distance gives a measure of convexity of the interface, with a more convex interface for larger numbers of this ratio (Fig. 3D). A more convex interface can hold a larger volume of water in the lens for a given lens thickness. The ratio shows a decreasing trend for increasing flux ratios, with a horizontal asymptote given by  $\ln(2)$ . Therefore, with an increase in flux ratio, the storage of recharge water decreases not only due to a decrease in maximum thickness, but also due to a decrease in convexity of the interface. This is also a main explanation for the more strongly increasing average residence times for flux ratios decreasing below 0.5 (Fig. 3A).

For the purpose of comparison, also the ratio of lens area divided by thickness is shown for the situation described by Maas (2007). It shows that, for a given maximum interface depth, the volume of water stored in the lens in an oceanic island is higher than for our current conditions. This may have implications for analyses in other work (Eeman et al., 2011; Stofberg et al., 2017), which apply the solution of Maas (2007) to problems which actually involve the domain as presented in this paper.

## 5. Transient flow

### 5.1. Mathematical model description

Even though the stream function (29) responds instantaneously to changes in boundary fluxes for an incompressible fluid, this does not imply that the interface does so as well. Rather, the interface moves along with the local velocity at the interface itself, which does respond instantaneously to changes. As such, in case of transient boundary fluxes, i.e.  $N(t)$ ,  $K(t)$ , the interface is no longer necessarily situated at the position where the stream function equals zero, and (21) no longer holds.

In the transient case, we obtain an equation for the movement of the interface by considering the seepage water balance in  $\mathcal{S}_K$ . It reads

$$\eta \frac{\partial I}{\partial t} + \frac{\partial}{\partial x} Q_s(x, t) = K(t), \quad (41)$$

where  $Q_s$  is the horizontal seepage water flux

$$Q_s(x, t) = \int_{-\infty}^{I(x,t)} q_x(x, y, t) dy. \quad (42)$$

In terms of the stream function, (42) becomes

$$Q_s(x, t) = \psi(x, -\infty, t) - \psi(x, I(x, t), t) = K(t)x - \psi(x, I(x, t), t). \quad (43)$$

Substitution of (43) in (41) yields the interface motion equation (Chan Hong et al, 1989)

$$\eta \frac{\partial I(x, t)}{\partial t} = \frac{\partial}{\partial x} \{ \psi(x, I(x, t), t) \} \quad (44)$$

subject to the initial condition  $I(x, 0) = I_{init}(x)$ . As the stream function reacts instantaneously to changes in the boundary fluxes, the right hand side term in (44) follows directly from (29) for situations without density differences. Clearly, the solution to (44) depends on the nature of  $N(t)$  and  $K(t)$ , such that no single unique answer exist.

We may reformulate the interface motion equation into its dimensionless equivalent. For this, we define the reference values

$$x_R = L; \quad \psi_R = N_0 L; \quad T_R = T, \quad (45)$$

where  $N_0$  is characteristic recharge rate, for instance an average recharge rate, and  $T$  is a characteristic time scale, for instance an oscillation period in case of sinusoidal boundary fluxes. Let us write any scaled parameter as e.g.  $\hat{x} = \frac{x}{x_R}$ . Using this notation, the interface motion equation (44) is written as

$$\eta \frac{x_R}{T_R} \frac{\partial \hat{I}}{\partial \hat{t}} = \frac{\psi_R}{x_R} \frac{\partial}{\partial \hat{x}} \hat{\psi}(\hat{x}, \hat{I}, \hat{t}) \quad \text{or} \quad \frac{\partial \hat{I}}{\partial \hat{t}} = \frac{\psi_R T_R}{\eta x_R^2} \frac{\partial}{\partial \hat{x}} \hat{\psi}(\hat{x}, \hat{I}, \hat{t}). \quad (46)$$

Substituting the reference values (45) in (46) yields the dimensionless interface motion equation

$$\frac{\partial \hat{I}}{\partial \hat{t}} = \varepsilon \frac{\partial}{\partial \hat{x}} \{ \hat{\psi}(\hat{x}, \hat{I}, \hat{t}) \}, \quad (47)$$

where we introduced the dimensionless parameter  $\varepsilon = \frac{N_0 T}{\eta L}$ . For further analyses, we implemented a numerical solution scheme to solve (47) using the Runge-Kutta method in time and central differences in space.

In order to provide additional insights into this transient problem, we consider an example where the boundary fluxes follow a sinusoidal pattern. Such sinusoidal boundary conditions may be relevant when seasonality in both recharge and seepage fluxes occurs. The example problem is given by

$$\begin{aligned} N(t) &= N_0 + A \sin\left(\frac{2\pi t}{T}\right) \\ K(t) &= K_0 - A \sin\left(\frac{2\pi t}{T}\right), \end{aligned} \quad (48)$$

where  $A$  [ $\text{LT}^{-1}$ ] is the flux amplitude,  $N_0$  and  $K_0$  [ $\text{LT}^{-1}$ ] are the average (positive) recharge and seepage fluxes, respectively, and  $T$  [T] is the reference period. Flux amplitude  $A$  may exceed both  $N_0$  and  $K_0$ , implying that  $N(t)$  and  $K(t)$  may become negative. This allows for seasonal evapotranspiration or downward seepage. Clearly, the parameters  $A$ ,  $N_0$  and  $K_0$  should be chosen such that  $I(x, t) < 0$  for  $0 \leq x < L$  and for all times  $t > 0$ . For this choice of boundary conditions, recharge decreases while seepage increases and vice versa, which resembles a real-world situation with a fixed aquifer head at sufficient distance from the groundwater table. In the summer period recharge may be low, such that phreatic groundwater levels are lower than heads in an underlying aquifer, resulting in increased upward seepage fluxes. Conversely, in winter more recharge results in higher phreatic groundwater levels, resulting in decreased upward seepage fluxes.

When (48) applies, the problem has two time-scales: the oscillation period  $T$  in the boundary conditions and the transport time  $\frac{\eta L}{N_0}$ . The ratio of the two,  $\varepsilon = \frac{N_0 T}{\eta L}$ , is the dimensionless parameter introduced in (47). When the oscillation period is much smaller than the transport time, i.e.  $\varepsilon \ll 1$ , we can follow van Duijn and van der Zee (2018) and apply a two-scale expansion to obtain an approximation of the time dependent interface behaviour. This approximation can be handled by analytical techniques when  $x = 0$ , i.e. at the location midway between the drains. The resulting expression is useful as benchmark for numerical simulations, and, more importantly, it gives insight in the roles of the two time scales. With  $h(t) := I(0, t)$  and  $h_{init} := h(0)$ , we derive in Appendix A the approximation

$$\begin{aligned} h(t) &= h_0(t) \\ &+ \varepsilon \frac{A}{N_0} \frac{L}{2\pi} \left( \cos\left(2\pi \frac{t}{T}\right) - \frac{1 + e^{\left(\frac{\pi h_{init}}{L}\right)}}{1 + e^{\left(\frac{\pi h_0(t)}{L}\right)}} e^{\frac{2N_0 + K_0}{2(N_0 + K_0)} \left(\frac{h_0(t)}{L} - \frac{h_{init}}{L} - \frac{K_0 t}{\eta L}\right)} \right) \\ &+ \mathcal{O}(\varepsilon^2), \end{aligned} \quad (49)$$

where  $\mathcal{O}(\varepsilon^2)$  [L] denotes the second and higher order terms with respect to  $\varepsilon$ . The function  $h_0(t)$  [L] is resolved from the algebraic equation

$$\begin{aligned} &\left| e^{\left(\frac{\pi h_0(t)}{L}\right)} - \frac{K_0}{2N_0 + K_0} \right| e^{\left(-\frac{2N_0 + K_0}{2(N_0 + K_0)} \frac{h_0(t)}{L}\right)} \\ &= \left| e^{\left(\frac{\pi h_{init}}{L}\right)} - \frac{K_0}{2N_0 + K_0} \right| e^{\left(-\frac{2N_0 + K_0}{2(N_0 + K_0)} \frac{h_{init}}{L}\right)} e^{\left(-\frac{K_0(2N_0 + K_0)}{2N_0(N_0 + K_0)} \frac{N_0 t}{\eta L}\right)}. \end{aligned} \quad (50)$$

In (49), the first term denotes the slow variation of the interface position. From (50) we deduce the following observations for the behaviour of  $h_0(t)$ :

- For any  $h_{init} < 0$ , and with  $h$  defined in (35),

$$\begin{aligned} h_0(t) &\rightarrow h \text{ as } t \rightarrow \infty, \text{ with exponential decay of order} \\ &\mathcal{O}\left(e^{\left(-\frac{K_0(2N_0 + K_0)}{2N_0(N_0 + K_0)} \frac{N_0 t}{\eta L}\right)}\right); \end{aligned}$$

- If  $h_{init} > h$ , then  $h_0(t)$  decreases towards  $h$ ;
- If  $h_{init} < h$ , then  $h_0(t)$  increases towards  $h$ ;

- If  $h_{init} = h$ , then  $h_0(t) = h$  for all  $t > 0$ .

The second term in (49) involving the cosine is  $\mathcal{O}(\varepsilon)$  and oscillates with period  $T$ . Since  $\varepsilon = \frac{N_0 T}{\eta L} \ll 1$ , this is the fast oscillating term. The third term in (49) is  $\mathcal{O}(\varepsilon)$  as well and denotes the slowly decaying correction to the first term  $h_0(t)$ .

If  $h_{init} = h_0$ , then (49) reduces to

$$h(t) = h_0 + \varepsilon \frac{A}{N_0} \frac{L}{2\pi} \left( \cos\left[2\pi \frac{t}{T}\right] - e^{\left(-\frac{K_0(2N_0 + K_0)}{2N_0(N_0 + K_0)} \frac{N_0 t}{\eta L}\right)} \right) + \mathcal{O}(\varepsilon^2). \quad (51)$$

As an example, we present solutions for time-dependent boundary conditions in the form of (48). We follow the development of the interface depth over time, based on (i) the analytical approximation (49), (ii) the numerical solution to the interface motion equation (47) and (iii) the first moment of the vertical concentration change midway between the drains as calculated with SUTRA. To obtain lens thickness from SUTRA simulation results, we used the average groundwater level over one period to avoid fast groundwater level fluctuations obscuring the slower movement of the interface: the groundwater level is highest in times of highest recharge rates and responds quite fast. If we would obtain lens thickness including these fast groundwater level movements, this would obscure the slower interface movement, in accordance with de Louw et al. (2013).

We describe three cases, which only deviate in their initial conditions (IC), and one additional case with a different ratio  $\varepsilon$  of the characteristic time  $T$  over the steady travel time  $\frac{\eta L}{N_0}$ . For the parameters not specifically mentioned in this section, we use reference parameters given in Table 1.

The initial conditions are given by the steady state solution for  $K/N$  ratios of 2, 1 and 0.5, respectively, of which their steady state solutions were already shown in Fig. 2. The transient boundary conditions are given by (48), with  $N_0 = K_0 = A = 0.5 \text{ mm d}^{-1}$ , and an oscillation period  $T$  of 364 days. Given (35) and (49), the interface position moves from an initial state (given as  $h/L$ ) of -0.22, -0.35 and -0.51, respectively, to an equilibrium at -0.35 for all three situations. The reference parameters give  $\varepsilon = 0.081$ . The fourth situation also starts at -0.22, but has a four times larger value of  $\varepsilon$  ( $\varepsilon = 0.324$ ) due to a decrease in porosity. As in our derivation of the analytical approximation we assumed  $\varepsilon \ll 1$ , this parameterization may be already quite extreme.

## 5.2. Example results

Calculated movement of the interface position midway between the drains by the analytical approximation (49), as given by the solid sinusoidal lines in Fig. 4, are hardly distinguishable from the numerical approximation of the interface motion equation (47) (dotted lines) at that position. The second and higher order terms in (49) therefore appear of minor importance and need not be evaluated for the given parameterization, even for the simulation with a higher value of  $\varepsilon$ . Results of our analytical approach also compare well to SUTRA (black dashed lines). There is a slight phase shift in the results of SUTRA as compared to our analytical approach. This may be caused by (i) a delay in response to changes in recharge due to the unsaturated zone, (ii) groundwater level fluctuations which are not accounted for in the analytical approximation, and (iii) oscillations in skewness of the mixing zone.

The second and third term in (49) are specific to the boundary conditions (48). The effect of the third term in (49) is clearly demonstrated for the situation with the initial condition given by  $K/N = 1$  (Fig. 4, in green). In the first few oscillation periods, the sinusoidal line lies below the solid, non-sinusoidal line for the majority of time. This is a consequence of the definition and timing of the initial – and boundary conditions. As the boundary conditions are defined such that  $N(t) > N_0$  and  $K(t) < K_0$  for  $0 < t < T/2$ , during this time the interface is pushed

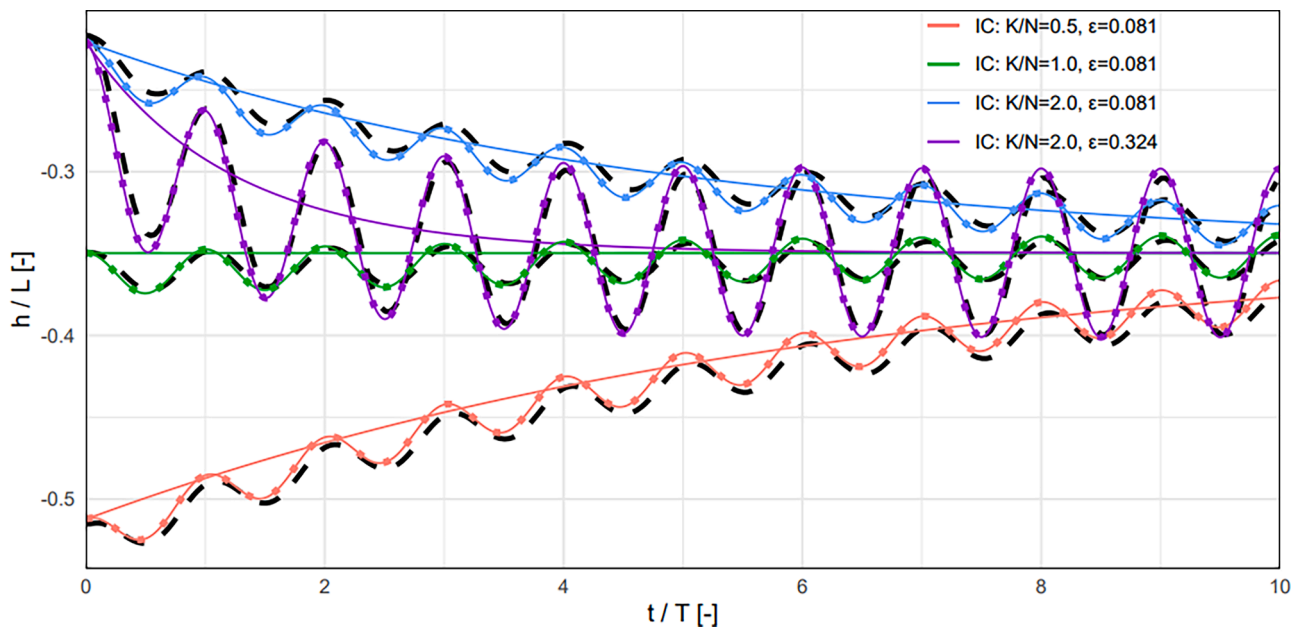


Fig. 4. Development of the interface depth midway between the drains, normalized by half a drain distance, as function of time, as obtained from the analytical approximation (49) (solid sinusoidal line), the numerical solution of the interface motion equation (47) (dotted sinusoidal line) and from SUTRA (black dashed lines), for differing initial conditions (IC) and/or ratios of the oscillation period over transport time ( $\epsilon$ ). The slow part of the analytical approximation  $h_0(t)/L$  (50) is depicted by the non-sinusoidal solid lines and can only be determined from the analytical approximation.

downward from its initial, steady state position, and in the remainder of this period the interface is pushed upward again, only to end up slightly above its initial condition. Therefore, most of the time within the first period the interface is below its starting position. The analytical results match the results of SUTRA of this correction closely.

The effect of the second term in (49) is apparent in all simulations. In the analytical approximation, the amplitude of the oscillations itself is not influenced by the initial condition, as seen directly from (49). It is solely driven by the value of  $\epsilon$  and changes in boundary fluxes, of which the latter directly influences the stream function in time. In the SUTRA model the groundwater table itself may fluctuate, implying that lens thickness not only changes due movement of solutes, but also due to changes in thickness of the saturated zone. This effect appears to have little influence on the amplitude of the oscillation of the interface itself. Thus, for the parameterizations chosen, the analytical model also compares well to the SUTRA model in this respect.

The first term in (49), as given by the solid non-sinusoidal lines describes the change in average interface position rather well when compared to SUTRA. This slow term movement may be of special interest, as it not only applies to our specific boundary conditions, but also applies to situations with a sudden change in boundary conditions or may be used to model the effects of gradual changes in boundary conditions.

Finally, Fig. 4 shows that the effect of an increase in the ratio of the oscillation period over steady travel time,  $\epsilon$ , is three-fold. (i) The amplitude of oscillations increases, (ii) the response time to changes in  $N_0$  and/or  $K_0$  decreases and (iii) the time required for the correction term to diminish is shortened. Hence, a hydrological system with a relatively large value of  $\epsilon$  is more sensitive to disturbances in boundary fluxes as compared to a system with smaller values of  $\epsilon$ . It seems that even with a relatively high value of  $\epsilon$  (0.324), the analytical approximation still aligns well with the numerical implementation of the interface motion equation as well as with SUTRA results. Hence, the contribution of the second and higher order terms in (49) remain small.

From the numerical implementation of the interface motion equation, we may not only derive the interface position midway between the drains, but also at any other location in  $0 < x < L$ . Obtaining the interface position sufficiently close to the drain, we may approximate

the angle of the interface close to the drain with this numerical implementation. With (34), this angle provides the relative contribution of both water sources (recharge and seepage) to discharge from the drain at any time  $t$ . Knowing the solute concentrations of both sources of water and the discharge volume, this relative contribution is easily converted to an estimate of concentration of the discharge water as well as solute load. SUTRA does, in itself, not distinguish between source of water, but with known input concentrations in the seepage and recharge water, we may use the model output of discharge volume and solute load to obtain an estimate of the relative contribution of both water sources to discharge at any time  $t$ .

A comparison with estimates of the relative contribution obtained from the angle of the interface close to the drain with those obtained from SUTRA is shown in Fig. 5, for the same situations as described in Fig. 4. The resemblance between both models is remarkable, considering that SUTRA also takes mixing of solutes into account. The amplitude of the oscillation obtained with SUTRA is slightly larger compared to the amplitude obtained from the interface motion equation, but patterns and the speed at which the equilibrium value of the oscillation changes are very similar. The difference in amplitude may be related to the fact that in SUTRA, discharge volume also shows a slight oscillating behaviour due to changes in the groundwater level, whereas discharge volume is constant in the interface motion equation for the given parameterization.

Clearly, the largest fluctuations in relative contribution, and thus solute concentration in the discharge water, are found for a larger value of  $\epsilon$ . Comparing the evolution of the concentration over time with that of the maximum lens thickness (Fig. 4), it is evident that the oscillations in concentration move towards their final equilibrium more rapidly in the early stages. This is a consequence of the fact that the interface close to the drain adjusts more rapidly to the new equilibrium boundary fluxes compared to the interface further away. As time proceeds, the slower adjustment of the interface further from the drain becomes the main driver of the rate at which the discharge concentration moves towards its final equilibrium oscillation. Consequently, this rate becomes more in line with the rate of change in maximum lens thickness.

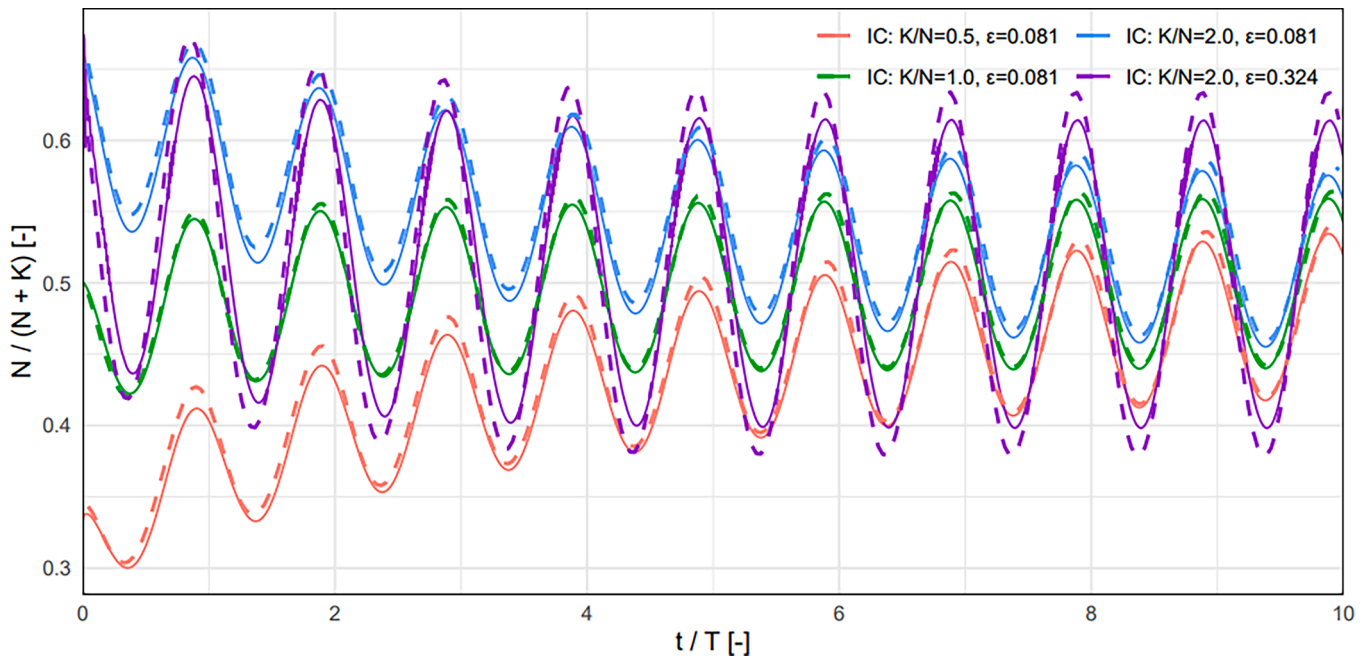


Fig. 5. Development of the contribution of the different types of water to the outflow at the drain, as obtained with the numerical implementation of the interface motion equation (47) sufficiently close to the drain and using (34) (solid lines) and with SUTRA (dashed lines), for differing initial conditions (IC) and/or ratios of the oscillation period over transport time ( $\epsilon$ ).

## 6. Mixing zone

### 6.1. Mathematical model description

In this section we construct a steady state approximation for the concentration in the diffusive-dispersive mixing zone midway between the drains; i.e. at  $x = 0$ . We use (3) and (6) at  $x = 0, y < 0$  as starting point. In (3) we assume the porosity and fluid density to be constant and we set  $q_x(0,y) = 0$ , in accordance with (30). Since the density is constant, we consider (3) in terms of the relative concentration  $C_r = \frac{w}{w_k}$ , such that

$0 \leq C_r \leq 1$ . In a very lengthy and technical derivation, detailed in Appendix B, we show that the concentration along the half-line  $\{(x, y): x = 0, y < 0\}$  satisfies approximately, with  $C_r(y) = C_r(0,y)$  for brevity,

$$\frac{d}{dy} \left( \left( \frac{\alpha_L |q_y(0,y)|}{\eta} + D_m \right) \frac{dC_r}{dy} \right) - \frac{q_y(0,y)}{\eta} \frac{dC_r}{dy} = 0 \text{ for } -\infty < y < 0, \tag{52}$$

subject to the boundary conditions  $C_r(0) = 0$  and  $C_r(-\infty) = 1$ .

Using the vertical flow velocity at  $x = 0$  (36), (52) can be solved for

Table 2  
Expressions for constants and functions used in (54) and (56).

Parameter	Expression	Unit
$A_1$	$= \frac{L}{(\alpha_L(2N+K) + \eta D_m)(\alpha_L K - \eta D_m)}$	-
$A_2$	$= \frac{2L}{\pi} \frac{(N+K)\eta D_m}{(\alpha_L(2N+K) + \eta D_m)(\alpha_L K - \eta D_m)}$	-
$A_3$	$= -\frac{1}{K(2N+K)} \left( \frac{K}{2N+K} \right)^{\frac{A_1}{\pi}} \left( \eta D_m \frac{N+K}{K} \sqrt{\frac{K}{2N+K}} \right)^{-A_2}$	$TL^{-1} T^{A_2} L^{2A_2}$
$a_1$	$= 1$	-
$a_2$	$= -\frac{L}{\pi} \frac{(2N+K)}{(\alpha_L(2N+K) + \eta D_m)}$	-
$a_3$	$= 1 - \frac{L}{\pi} \frac{K}{(\alpha_L K - \eta D_m)}$	-
$a_4(y)$	$= \frac{\alpha_L(2N+K) + \eta D_m}{\alpha_L K - \eta D_m} e^{\frac{\pi y}{L}}$	-
$B_1$	$= \frac{L}{(\alpha_L(2N+K) + \eta D_m)(\alpha_L K - \eta D_m)}$	-
$B_2$	$= \frac{2L}{\pi} \frac{(N+K)\eta D_m}{(\alpha_L(2N+K) + \eta D_m)(\alpha_L K - \eta D_m)}$	-
$B_3$	$= \frac{1}{K(2N+K)} \left( \frac{K}{2N+K} \right)^{-\frac{B_1}{\pi}} \left( -\eta D_m \frac{N+K}{K} \sqrt{\frac{K}{2N+K}} \right)^{-B_2}$	$TL^{-1} T^{A_2} L^{2A_2}$
$b_1$	$= 1$	-
$b_2$	$= \frac{L}{\pi} \frac{(2N+K)}{(\alpha_L(2N+K) - \eta D_m)}$	-
$b_3$	$= 1 + \frac{L}{\pi} \frac{K}{(\alpha_L K + \eta D_m)}$	-
$b_4(y)$	$= \frac{\alpha_L(2N+K) - \eta D_m}{\alpha_L K + \eta D_m} e^{\frac{\pi y}{L}}$	-

$C_r$  (Appendix B) by considering the region below and above the interface position at  $x = 0$  individually, following the observations in (37). Below the interface we obtain

$$C_r(y) = 1 + J(h) \operatorname{Re}[B(y)] \text{ for } -\infty < y < h, \quad (53)$$

with

$$B(y) = B_3 e^{B_1 \frac{y}{L}} (-K + 2(N + K) F(b_1, b_2; b_3; b_4(y))) \left( (\alpha_L N - \eta D_m) \cosh\left(\frac{\pi y}{2L}\right) + \alpha_L (N + K) \sinh\left(\frac{\pi y}{2L}\right) \right)^{B_2}. \quad (54)$$

where  $J(h)$  [ $LT^{-1}$ ] is the (at this point unknown) diffusive salt flux at the interface and  $F(b_1, b_2; b_3; b_4(y))$  the hypergeometrical function (e.g. Abramowitch and Stegun, 1964). Further,  $B_i$  and  $b_i$  ( $i = 1, 2, 3$ ) are constants and  $b_4(y)$  is a function of  $y$ . They are specified in Table 2. We take the real part of  $B(y)$  in (53) because some of the powers in  $B(y)$  may be negative.

For the region above the interface, we obtain

$$C_r(y) = 1 + J(h) \operatorname{Re}[A(y) + B(h) - A(h)] \text{ for } h < y < 0, \quad (55)$$

with

$$A(y) = A_3 e^{-A_1 \frac{y}{L}} (K - 2(N + K) F(a_1, a_2; a_3; a_4(y))) \left( (\alpha_L N + \eta D_m) \cosh\left(\frac{\pi y}{2L}\right) + \alpha_L (N + K) \sinh\left(\frac{\pi y}{2L}\right) \right)^{A_2}. \quad (56)$$

The constants  $A_i$  and  $a_i$  ( $i = 1, 2, 3$ ) and the function  $a_4(y)$  are given in Table 2. The flux at the interface is obtained from the condition  $C_r(0) =$

0:

$$J(h) = \frac{1}{\operatorname{Re}[A(0) + B(h) - A(h)]}. \quad (57)$$

Expressions (53) - (57) are derived in a dimensionless setting in Appendix B. It was found that, in the end, the characteristic dimensionless numbers that remain are  $D^*$ ,  $\alpha_L^*$  and  $K^*$ , given as

$$D^* = \frac{\eta D_m}{\alpha_L N} \text{ and } \alpha_L^* = \frac{\alpha_L}{L} \text{ and } K^* = \frac{K}{N}. \quad (58)$$

### 6.2. Example results

Concentration profiles in the vertical direction midway between the drains compare well between the analytical and numerical steady state solutions, especially below the interface position (Fig. 6). Above the interface, the mixing zone obtained with the numerical model extends slightly further towards the groundwater table. Two main reasons for this are (i) the fact that in the numerical model, solutes are allowed to

enter the unsaturated zone, whereas in the analytical model we assume the concentration to be zero at  $y = 0$ , and (ii) the upward curvature of the interface, and thus also the mixing zone, moving away from the position midway between drains. The latter implies that especially

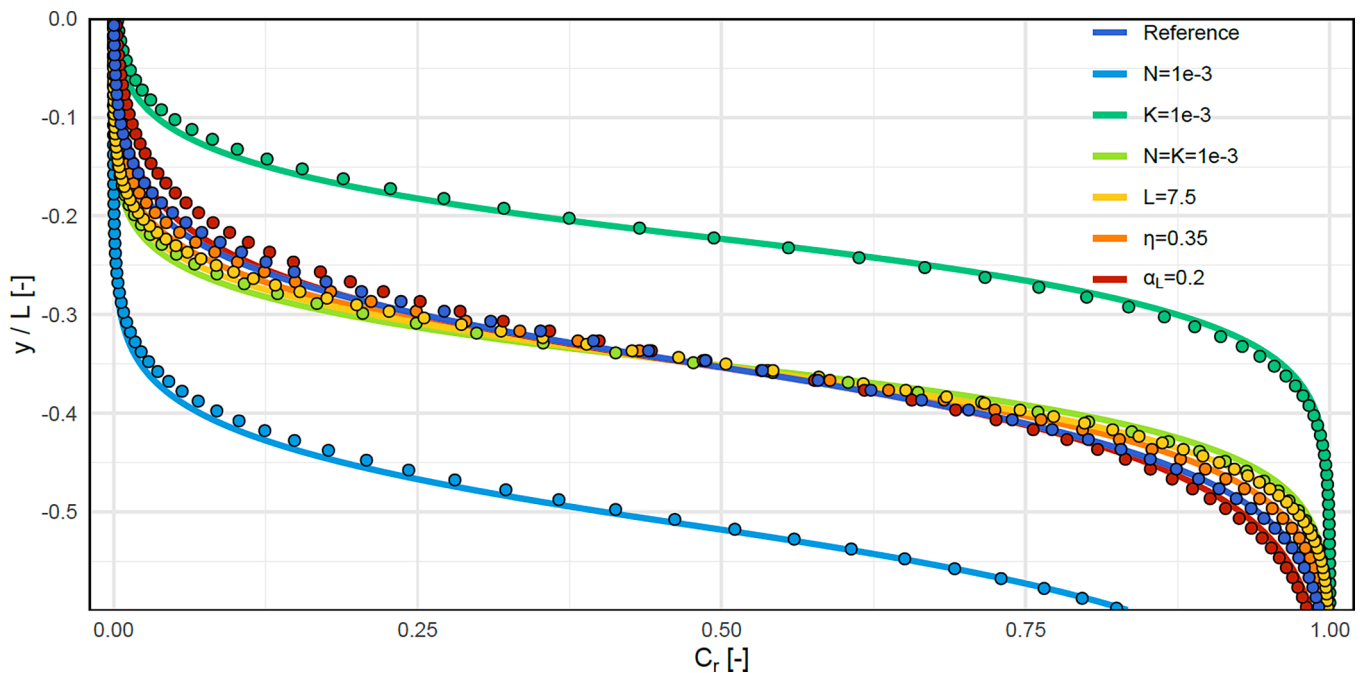
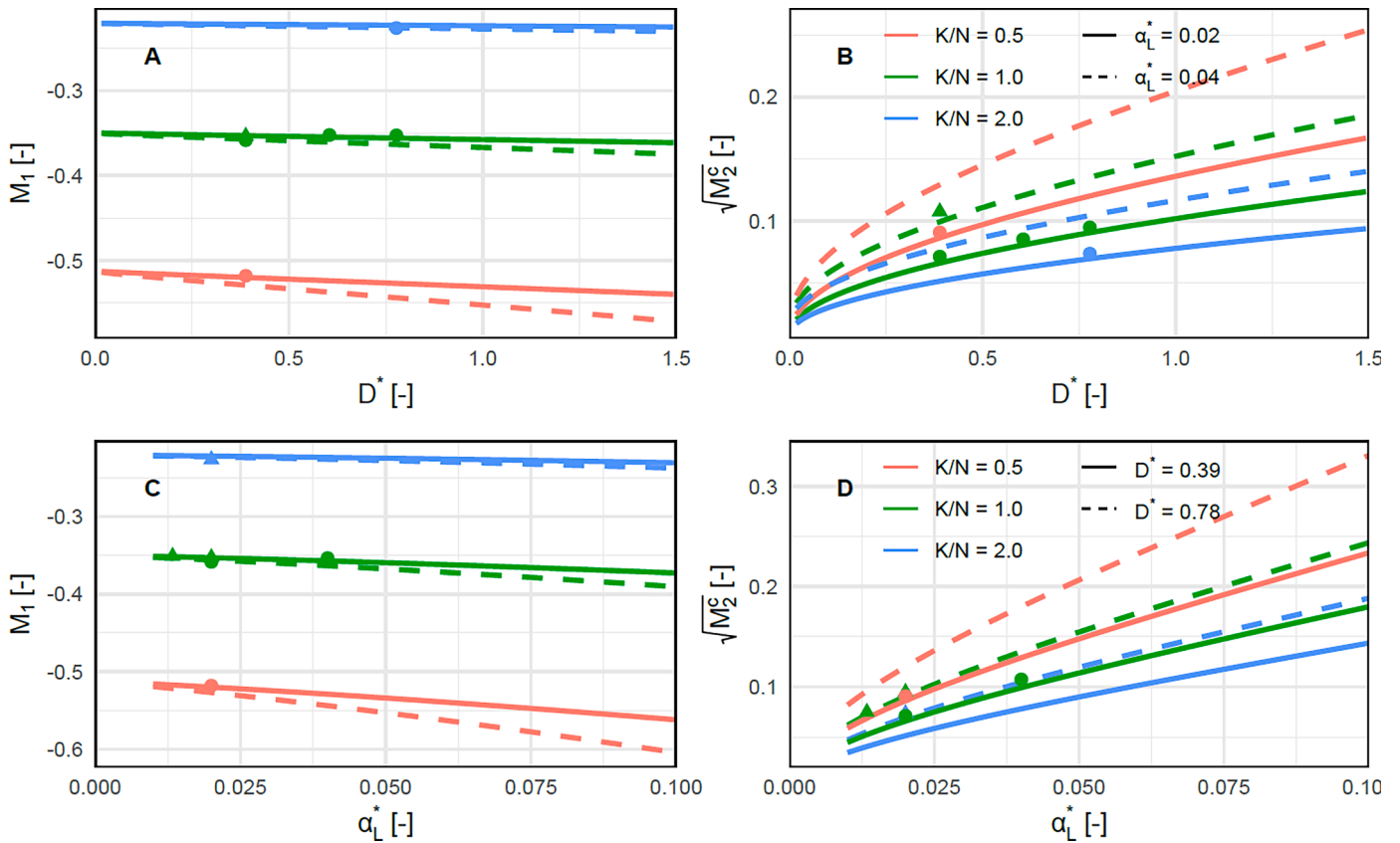


Fig. 6. Relative concentration in the vertical direction midway between the drains. Lines indicate analytical results, dots represent numerical SUTRA simulations. Colors indicate results for the reference simulation (dark blue), and simulations in which one or two parameters are altered with respect to the reference, as indicated in the legend.



**Fig. 7.** (A) Dimensionless first moment ( $M_1$ ) of the vertical concentration gradient midway between the drains as function of  $D^*$ .  $M_1$  provides an estimate of the interface position. Colors indicate the flux ratio, line type indicates the value of  $\alpha_L^*$ , and dots or triangles give the moments of the numerical SUTRA simulations given in Fig. 6 for  $\alpha_L^* = 0.02$  and  $\alpha_L^* = 0.04$ , respectively. (B) Dimensionless square root of the second central moment ( $M_2$ , right panel), providing a measure of mixing zone thickness. Symbology as in (A). (C) As (A), but now  $M_1$  is plotted as function of  $\alpha_L^*$ , and line type shows two values of  $D^*$ . Dots and triangles give the moments of the numerical SUTRA simulations for  $D^* = 0.39$  and  $D^* = 0.78$ , respectively. (D) As (B), with symbology as in (c).

above the interface, mixing in the horizontal direction, which was deemed small in the analytical approach, and was ignored correspondingly, may result in some additional dispersion and spreading of the mixing zone.

Fig. 6 shows the effects of changes of values of individual parameters. The effects on the mixing zone shape and extent are similar in both the numerical and analytical approach. These effects may also be interpreted in light of the dimensionless groups  $D^* = \frac{\eta D_m}{\alpha_L N^*}$ ,  $\alpha_L^* = \frac{\alpha_L}{L}$  and  $K^* = \frac{K}{N}$ . A simultaneous increase in recharge and seepage rate, as well as a decrease in porosity, only affect  $D^*$  and both do so by reducing its value. As a consequence the mixing zone width decreases (Fig. 6). An increase in drain distance affects only  $\alpha_L^*$ , resulting in a (relative) decrease in mixing zone thickness as well. The dispersion length influences both  $D^*$  and  $\alpha_L^*$ , and does so in an opposite direction. For the parameterization in Fig. 6, an increase in dispersion length results in an increase in mixing zone width as compared to the reference case, hence, for these parameters the effect of  $\alpha_L^*$  is dominant over  $D^*$ . An increase in seepage rate, and thus only an increase in  $K^*$ , leads to a decrease of the mixing zone width. Finally, an increase in recharge rate, reducing both  $K^*$  and  $D^*$ , also results in a decrease in mixing zone width, which is less pronounced as compared to the decrease with a change in seepage rate. We therefore conclude that  $D^*$  is dominant over  $K^*$  for the chosen parameters.

These examples demonstrate the importance of individual parameters on the behavior of the mixing zone. We may also examine the response of the average mixing zone position (first moment) and width (as root of the second central moment) upon changes in the dimensionless groups  $D^*$ ,  $\alpha_L^*$  and  $K^*$ . The first moment of the mixing zone as obtained with the analytical approximation presented here is given in

Figs. 7A and C, for varying combinations of the dimensionless groups. For increasing values of  $D^*$  and  $\alpha_L^*$ , the first moment is situated deeper in the soil profile, and this effect is more pronounced for lower flux ratios. The reason for this shift is that the mixing zone spreads further into the seepage water part compared to the recharge water part; thus, the mixing zone becomes negatively skewed. This is a consequence of both the flow pattern and the solute boundary conditions, with higher velocity gradients in the recharge water part, and a prescribed concentration at  $y = 0$ . Also note that for  $D^* = \alpha_L^* = 0$ , the first moment coincides exactly with the interface position as obtained with the sharp interface approximation. For any  $\alpha_L^* > 0$  and  $D^* > 0$ , the first moment is situated lower in the domain.

With respect to the mixing zone width, for which we take the square root of the second central moment, we see in Fig. 7B and D the following general behaviour. For increasing values of  $D^*$  and  $\alpha_L^*$  the mixing zone width becomes larger. The width is smaller for increasing flux ratios, which is a consequence of the higher velocity gradients when the lens becomes shallower due to the increase in flux ratio. The numerical SUTRA results agree with these analytical results, although the obtained widths are consistently somewhat higher than obtained with the analytical model. This was observed in Fig. 6 as well.

### 7. Conclusions

In this Part 1 of a series of two papers on flow in shallow water lenses subject to upward seepage and downward infiltration of recharge, we have obtained analytical expressions for steady state, transient and mixing zone problems, for the situation without density differences between the two types of water. Using the sharp interface approach, we

have obtained an expression for the stream function in steady state, from which we obtain the interface between the two types of water, being either recharge or seepage water. This allows us to also calculate travel times of water in the shallow water lens, depending on the entrance location of water.

For transient conditions, we obtained the interface motion equation, which can be solved by simple numerical techniques along the entire horizontal width of the domain. For a situation with specific oscillatory boundary conditions, we have demonstrated that the interface position midway between the drains can be handled accurately by analytical techniques. This allows for a simple evaluation of how parameters as porosity and drain distance affect the response of the interface upon changes in boundary conditions. The interface motion equation may also be used to estimate the relative contribution of both water sources to drain discharge at any moment in time.

Finally, we developed an analytical approximation of the mixing zone in the vertical direction midway between the drains for steady state conditions. Based on this analysis we have identified three dimensionless parameter groups which determine the front width, which improves our understanding of the interaction between factors determining the mixing zone thickness.

For all cases, we have shown that the results of our analytical expressions align very well with numerical model results of the model SUTRA, which solves convection, dispersion and diffusion in the two dimensions considered. The analytical expressions provided in this paper provide much more conceptual understanding of the flow of water and solutes in shallow water lenses as compared to numerical models, allows for simple exploration of the sensitivity of the shallow lenses to changing conditions, and may provide a basis for further studies on this

## Appendix A. – Derivation of the transient approximation

In this appendix we derive (49) and (50), which correspond to the dimensionless Eqs. (A.25) and (A.20) below. Again, we drop the ‘hat’ from the dimensionless notation. In this setting, boundary conditions (48) become

remove this equation

$$\begin{aligned} N(t) &= 1 + A\sin(2\pi t) \\ K(t) &= K - A\sin(2\pi t) \end{aligned} \quad (\text{A.1})$$

where  $A$  denotes the dimensionless amplitude and where  $K := K_0/N_0$  is the ratio of upward seepage and recharge.

We implement these boundary conditions in the steady state formulation of the stream function (29) to obtain

$$\psi(x, y, t) = (K - A\sin(2\pi t))x - (1 + K)u(x, y), \quad (\text{A.2})$$

with  $u(x, y)$  given by (28). Note that  $u(x, y)$  itself is, conveniently, independent of the boundary fluxes. Substitution of (A.2) into the dimensionless interface motion equation (47) yields the interface motion equation specific for the boundary conditions (A.1):

$$\frac{\partial I}{\partial t} = \varepsilon \left( K - A\sin(2\pi t) - (1 + K) \frac{\partial}{\partial x} (u(x, I)) \right), \quad (\text{A.3})$$

subject to the initial condition  $I(x, 0) = I_{init}(x)$ . Here  $\varepsilon = \frac{N_0 T}{\eta L}$  is assumed to be a small parameter, so that a slow and fast timescale can be distinguished, according to

$$\tau = \varepsilon t \text{ and } s = \frac{\tau}{\varepsilon} = t \quad (\text{A.4})$$

respectively. This allows us to write (A.3) as

$$\frac{\partial I}{\partial \tau} = \underline{K - (1 + K) \frac{\partial}{\partial x} \{u(x, I)\}} - A\sin(2\pi s). \quad (\text{A.5})$$

The underlined part in (A.5) indicates the slow part, independent of  $s$ . To obtain a solution to (A.5), we consider a two-scale expansion of  $I(x, \tau)$ , for  $\tau > 0$  and  $0 < s < 1$ , see e.g. van Duijn and van der Zee (2018). This approximation is of the form

$$I(x, \tau) = I_0(x, \tau, s) + \varepsilon I_1(x, \tau, s) + \varepsilon^2 I_2(x, \tau, s) + \dots, \quad (\text{A.6})$$

subject.

## CRediT authorship contribution statement

**D. van de Craats:** Conceptualization, Methodology, Software, Formal analysis, Writing – original draft, Visualization. **C.J. van Duijn:** Writing – original draft, Methodology, Conceptualization. **P.A.C. Raats:** Writing – original draft, Methodology.

## Declaration of competing interest

The authors declare that they have no known competing financial interests or personal relationships that could have appeared to influence the work reported in this paper.

## Data availability

No data was used for the research described in the article.

## Acknowledgements

This research in the context of the project Water Nexus is financed by the Netherlands Organization for Scientific Research (NWO) under Contract no. 14299, which is partly funded by the Ministry of Economic Affairs and Climate Policy, and co-financed by the Netherlands Ministry of Infrastructure and Water Management and partners of the Dutch Water Nexus consortium.

where  $I_i$  for  $i = 0, 1, 2, \dots$  is 1-periodic with respect to  $s$  and where  $I_0(x, 0, 0) = I_{mit}(x)$  and  $I_i(x, 0, 0) = 0$  for  $i = 1, 2, \dots$ . When we differentiate  $I(x, \tau)$  on the left hand side in (A.6) in  $\tau$ , we differentiate the right hand side terms in (A.6) in  $\frac{\partial}{\partial \tau} + \frac{1}{\epsilon} \frac{\partial}{\partial s}$ . We may then substitute (A.6) into (A.5) to obtain

$$\frac{\partial I_0}{\partial \tau} + \frac{1}{\epsilon} \frac{\partial I_0}{\partial s} + \epsilon \frac{\partial I_1}{\partial \tau} + \frac{\partial I_1}{\partial s} + \epsilon^2 \frac{\partial I_2}{\partial \tau} + \epsilon \frac{\partial I_2}{\partial s} + \dots = K - (1 + K) \frac{\partial}{\partial x} \left\{ u(x, I_0) + \epsilon \frac{\partial u}{\partial y}(x, I_0) I_1 + \mathcal{O}(\epsilon^2) \right\} - A \sin(2\pi s). \tag{A.7}$$

If we consider the powers of  $\epsilon$  in (A.7), we find

$$\begin{aligned} \text{i. } \epsilon^{-1} & : \frac{\partial I_0}{\partial s} = 0 \\ \text{ii. } \epsilon^0 & : \frac{\partial I_0}{\partial \tau} + \frac{\partial I_1}{\partial s} = K - (1 + K) \frac{\partial}{\partial x} \{u(x, I_0)\} - \underline{A \sin(2\pi s)} \\ \text{iii. } \epsilon^1 & : \frac{\partial I_1}{\partial \tau} + \frac{\partial I_2}{\partial s} = -(1 + K) \frac{\partial}{\partial x} \left\{ \frac{\partial u}{\partial y}(x, I_0) I_1 \right\} \end{aligned} \tag{A.8}$$

Clearly, (i) implies that  $I_0$  is a function of only  $x$  and  $\tau$  and not of  $s$ , implying that the lowest order term is independent of the fast timescale. The underlined terms in (ii) are 1-periodic in  $s$ . Hence, integration of (ii) from  $s = 0$  to  $s = 1$  yields

$$\frac{\partial I_0}{\partial \tau} = K - (1 + K) \frac{\partial}{\partial x} \{u(x, I_0)\}, \tag{A.9}$$

with  $I_0(x, 0) = I_{mit}(x)$ . As  $u(x, I_0)$  is known from (28), this gives us, in principle,  $I_0(x, \tau)$ .

We also see from (ii) in (A.8) that

$$\frac{\partial I_1}{\partial s} = -A \sin(2\pi s) \text{ or } I_1 = \frac{A}{2\pi} \cos(2\pi s) + g(x, \tau) \tag{A.10}$$

for  $0 < s < 1$ , where  $g(x, \tau)$  is an unknown integration constant which needs to be determined. Since  $I_1(x, 0, 0) = 0$ , given as initial condition,  $g(x, 0) = -A/2\pi$ . An equation for  $g(x, \tau)$  is found by substituting (A.10) into (A.8 iii). This gives

$$\frac{\partial g}{\partial \tau} + \frac{\partial I_2}{\partial s} = -(1 + K) \frac{\partial}{\partial x} \left\{ \frac{\partial u}{\partial y}(x, I_0) \left( \frac{A}{2\pi} \cos(2\pi s) + g(x, \tau) \right) \right\}. \tag{A.11}$$

The underlined terms again denote the parts which are 1-periodic in  $s$ . Also recall that  $I_0$  is a function of only  $x$  and  $\tau$ . Integrating (A.11) from  $s = 0$  to  $s = 1$  yields

$$\frac{\partial g}{\partial \tau} = -(1 + K) \frac{\partial}{\partial x} \{a g(x, \tau)\}, \tag{A.12}$$

where  $a(x, \tau) = \frac{\partial u}{\partial y}(x, I_0(x, \tau))$ . This is a first order hyperbolic equation, with a characteristic speed given by  $(1 + K)a$ . Since  $u(0, y) = u(1, y) = 0$  for all  $y < 0$  (see (25)), it follows that  $a(0, \tau) = a(1, \tau) = 0$  as well. This implies that the characteristics are in the  $\tau$  direction at  $x = 0$  and  $x = 1$ , and thus no boundary conditions are required in (A.12) (nor in (A.9)).

Summarizing, we now have obtained the expansion

$$I(x, \tau) = I_0(x, \tau) + \epsilon \left( \frac{A}{2\pi} \cos\left(2\pi \frac{\tau}{\epsilon}\right) + g(x, \tau) \right) + \mathcal{O}(\epsilon^2) \tag{A.13}$$

for  $0 < x < 1$  and  $\tau > 0$ . This essentially gives us an expression for the interface with slow and fast terms:  $I_0(x, \tau)$  describes to leading order the slow movement of the interface, the term  $\epsilon g(x, \tau)$  denotes a first order correction to  $I_0$  and  $\frac{\epsilon A}{2\pi} \cos\left(2\pi \frac{\tau}{\epsilon}\right)$  is the fast oscillatory term due to the boundary conditions.

To evaluate (A.13) at each position between the drains, i.e. for arbitrary  $0 \leq x < L$ , is not straightforward. Fortunately, the situation simplifies midway between the drains, in the sense that at  $x = 0$ , Eqs. (A.9) and (A.12) can be handled by analytical techniques. The key point is that at  $x = 0$  (see (25)),

$$u(0, y) = 0 \text{ for all } y < 0. \tag{A.14}$$

Hence,

$$\frac{\partial u}{\partial y}(0, y) = 0, \frac{\partial^2 u}{\partial y^2}(0, y) = 0 \text{ for all } y < 0. \tag{A.15}$$

Evaluating

$$\frac{\partial}{\partial x} \{u(x, I_0)\} = \frac{\partial u}{\partial x}(x, I_0) + \frac{\partial u}{\partial y}(x, y) \frac{\partial I_0}{\partial x}$$

at  $x = 0$ , then gives

$$\frac{\partial}{\partial x} \{u(x, I_0)\}|_{x=0} = \frac{\partial u}{\partial x}(0, I_0). \tag{A.16}$$

Next we introduce the notation

$$h(\tau) := I(0, \tau) \text{ and } h_0(\tau) := I_0(0, \tau). \tag{A.17}$$

Using (28) or (32) in (A.16) and (A.9), yields for  $h_0$  the initial value problem

$$\begin{cases} \frac{\partial h_0}{\partial \tau} = K - 2(1+K) \frac{e^{\pi h_0}}{1+e^{\pi h_0}} \text{ for } \tau > 0 \\ h_0(0) = I_{init}(0) \end{cases}. \tag{A.18}$$

To solve this problem, first rewrite (A.18) as

$$\frac{\partial h_0}{\partial \tau} = -(2+K) + 2(1+K) \frac{1}{1+e^{\pi h_0}}.$$

Multiplying both sides by  $e^{\pi h_0}$ , we find for  $w = e^{\pi h_0}$

$$\frac{1}{\pi} \frac{\partial w}{\partial \tau} = -(2+K)w + 2(1+K) \frac{w}{1+w},$$

or

$$\frac{1+w}{Kw - (2+K)w^2} \frac{\partial w}{\partial \tau} = \pi$$

or

$$\left( \frac{1}{w} - \frac{2(1+K)}{2+K} \frac{1}{w - \frac{K}{2+K}} \right) \frac{\partial w}{\partial \tau} = \pi K.$$

Straightforward integration yields

$$\left( \frac{|w(\tau) - \frac{K}{2+K}|^{\frac{2(1+K)}{2+K}}}{w(\tau)} \right) = \left( \frac{|w(0) - \frac{K}{2+K}|^{\frac{2(1+K)}{2+K}}}{w(0)} \right) e^{-\pi K \tau}. \tag{A.19}$$

In terms of  $h_0$  this reads as

$$\left| e^{\pi h_0(\tau)} - \frac{K}{2+K} \right| e^{-\frac{2+K}{2(1+K)} \pi h_0(\tau)} = \left| e^{\pi I_{init}(0)} - \frac{K}{2+K} \right| e^{-\frac{2+K}{2(1+K)} \pi I_{init}(0)} e^{-\frac{K(2+K)}{\pi 2(1+K)} \tau}. \tag{A.20}$$

Clearly, if  $I_{init} = \frac{1}{\pi} \ln\left(\frac{K}{2+K}\right)$ , then  $h_0(\tau) = \frac{1}{\pi} \ln\left(\frac{K}{2+K}\right)$  for all  $\tau > 0$ , and

$$h_0(\tau) \rightarrow \frac{1}{\pi} \ln\left(\frac{K}{2+K}\right) \text{ as } \tau \rightarrow \infty \text{ for any } I_{init}(0) < 0, \tag{A.21}$$

with exponential decay.

Next we consider (A.12). In this equation

$$a(x, \tau) = \frac{\partial u}{\partial y}(x, I_0(x, \tau))$$

and

$$\frac{\partial a}{\partial x} = \frac{\partial^2 u}{\partial x \partial y}(x, I_0) + \frac{\partial^2 u}{\partial y^2}(x, I_0) \frac{\partial I_0}{\partial x}.$$

At  $x = 0$ , we apply (A.15) yielding

$$a(0, \tau) = 0 \text{ and } \frac{\partial a}{\partial x}(0, \tau) = \frac{\partial^2 u}{\partial x \partial y}(0, I_0).$$

Cross differentiating (28) and using the notation from (A.17) and  $g(\tau) = g(0, \tau)$ , we obtain at  $x = 0$  the problem

$$\frac{\partial g}{\partial \tau} = -2\pi(1+K) \frac{\exp(\pi h_0)}{(1 + \exp(\pi h_0))^2} g \text{ for } \tau > 0, \tag{A.22}$$

with  $g(0) = -A/2\pi$ .

Using (A.18) we write (A.22) as

$$\begin{aligned}\frac{1}{g} \frac{\partial g}{\partial \tau} &= \pi \left( \frac{\partial h_0}{\partial \tau} - K \right) \frac{1}{1 + e^{\pi h_0}} \\ &= \pi \left( \frac{\partial h_0}{\partial \tau} - K \right) \left( 1 - \frac{e^{\pi h_0}}{1 + e^{\pi h_0}} \right) \\ &= \pi \frac{\partial}{\partial \tau} (h_0 - K\tau) - \pi \frac{e^{\pi h_0}}{1 + e^{\pi h_0}} \frac{\partial h_0}{\partial \tau} + \pi K \frac{e^{\pi h_0}}{1 + e^{\pi h_0}}\end{aligned}$$

Again with (A.18):

$$\frac{1}{g} \frac{\partial g}{\partial \tau} = \pi \frac{\partial}{\partial \tau} (h_0 - K\tau) - \pi \frac{e^{\pi h_0}}{1 + e^{\pi h_0}} \frac{\partial h_0}{\partial \tau} + \frac{\pi K}{2(1+K)} \frac{\partial}{\partial \tau} (h_0 - K\tau).$$

Thus, we have found:

$$\frac{\partial}{\partial \tau} \ln|g| = -\frac{\partial}{\partial \tau} \ln(1 + e^{\pi h_0}) + \frac{\pi(2+K)}{2(1+K)} \frac{\partial}{\partial \tau} (h_0 - K\tau)$$

or

$$g(\tau) = -\frac{A}{2\pi} \frac{1 + e^{\pi I_{init}(0)}}{1 + e^{\pi h_0(\tau)}} e^{-\frac{\pi(2+K)}{2(1+K)} \tau} (h_0(\tau) - I_{init}(0) - K\tau). \quad (\text{A.23})$$

Hence, we have obtained an explicit solution for  $g$  in terms of  $h_0$ .

Combining (A.23) and (A.21), it follows that

$$g(\tau) = \mathcal{O} \left( e^{-\frac{K(2+K)}{2(1+K)} \tau} \right) \text{ as } \tau \rightarrow \infty. \quad (\text{A.24})$$

The special case  $I_{init}(0) = \frac{1}{\pi} \ln \left( \frac{K}{2+K} \right)$  yields  $h_0 = \frac{1}{\pi} \ln \left( \frac{K}{2+K} \right)$  and thus

$$g(\tau) = -\frac{A}{2\pi} e^{-\frac{K(2+K)}{2(1+K)} \tau}.$$

To summarize: midway between the drains the interface behaves according to

$$h(\tau) = h_0(\tau) + \frac{\varepsilon A}{2\pi} \left( \cos \left( 2\pi \frac{\tau}{\varepsilon} \right) - \frac{1 + e^{\pi I_{init}(0)}}{1 + e^{\pi h_0(\tau)}} e^{\left( \frac{\pi(2+K)}{2(1+K)} (h_0(\tau) - I_{init}(0) - K\tau) \right)} \right) + \mathcal{O}(\varepsilon^2). \quad (\text{A.25})$$

The slow variable  $h_0(\tau)$  needs to be resolved from (A.20). The large time behaviour is

$$h(\tau) \rightarrow \frac{1}{\pi} \ln \left( \frac{K}{2+K} \right) + \frac{\varepsilon A}{2\pi} \cos \left( 2\pi \frac{\tau}{\varepsilon} \right) + \mathcal{O}(\varepsilon^2). \quad (\text{A.26})$$

## Appendix B. – Derivation of the mixing zone approximation

In this appendix we show the derivation of the mixing zone approximation. Starting point is the steady state form of the solute transport equation (3) where the density  $\rho$  and porosity  $\eta$  are assumed constant. For the solute mass fraction  $w$  [MM<sup>-1</sup>] results

$$\nabla \cdot (\rho w \vec{q}) = \nabla \cdot [\eta \rho (D_m \vec{I} + \vec{D}) \nabla w], \quad (\text{B.1})$$

In the domain between the drains  $(-L, L) \times (-\infty, 0)$ , subject to the horizontal boundary conditions

$$w(x, 0) = 0, \quad w(x, -\infty) = w_K \text{ for } -L < x < L. \quad (\text{B.2})$$

The conditions along the vertical boundaries  $\{x = \pm L\}$  are zero-flux, but they do not play a role in the analysis below. Redefining  $C_r := \frac{w}{w_K}$  and substituting in (B.1), now with boundary conditions

$$C_r(x, 0) = 0, \quad C_r(x, -\infty) = 1 \text{ for } -L < x < L, \quad (\text{B.3})$$

allows us (since  $\text{div } \vec{q} = 0$ ) to write (B.1) as

$$\vec{q} \cdot \nabla C_r = \nabla \cdot [\eta (D_m \vec{I} + \vec{D}) \nabla C_r], \quad (\text{B.4})$$

where  $\vec{q}$  is given by (30) and (31). We substitute  $\vec{q} = \eta \vec{v}$  in (B.4) in the remainder of this appendix.

To clarify the role of the various model parameters, let us first rescale the equation (as we did in Appendix A) by setting

$$\vec{v} = \frac{\eta}{N} \vec{v}, \quad \hat{x} = \frac{x}{L} \quad \text{and} \quad \hat{y} = \frac{y}{L}. \tag{B.5}$$

Then, from (30) and (31)

remove equation

$$\begin{aligned} \hat{v}_x &= (1 + K) \frac{\sin(\pi \hat{x})}{\cos(\pi \hat{x}) + \cosh(\pi \hat{y})} \\ \hat{v}_y &= - \left( 1 + (1 + K) \frac{\sinh(\pi \hat{y})}{\cos(\pi \hat{x}) + \cosh(\pi \hat{y})} \right) \end{aligned} \tag{B.6}$$

where  $K := K/N_0$  and  $N := N/N_0 = 1$ .

Further, (B.4) becomes

$$\hat{v}_x \frac{\partial C_r}{\partial \hat{x}} + \hat{v}_y \frac{\partial C_r}{\partial \hat{y}} = \frac{\alpha_L}{L} \frac{\partial}{\partial \hat{x}} \left( (d_{xx}(\hat{x}, \hat{y}) + D^*) \frac{\partial C_r}{\partial \hat{x}} + d_{xy}(\hat{x}, \hat{y}) \frac{\partial C_r}{\partial \hat{y}} \right) + \frac{\alpha_L}{L} \frac{\partial}{\partial \hat{y}} \left( d_{yx}(\hat{x}, \hat{y}) \frac{\partial C_r}{\partial \hat{x}} + (d_{yy}(\hat{x}, \hat{y}) + D^*) \frac{\partial C_r}{\partial \hat{y}} \right), \tag{B.7}$$

where

remove eq.

$$\begin{aligned} d_{xx}(\hat{x}, \hat{y}) &= \frac{|\hat{v}_x(\hat{x}, \hat{y})|^2 + \frac{\alpha_T}{\alpha_L} |\hat{v}_y(\hat{x}, \hat{y})|^2}{\vec{v}(\hat{x}, \hat{y})} \\ d_{yy}(\hat{x}, \hat{y}) &= \frac{\frac{\alpha_T}{\alpha_L} |\hat{v}_x(\hat{x}, \hat{y})|^2 + |\hat{v}_y(\hat{x}, \hat{y})|^2}{\vec{v}(\hat{x}, \hat{y})} \\ d_{xy}(\hat{x}, \hat{y}) &= d_{yx}(\hat{x}, \hat{y}) = \left( 1 - \frac{\alpha_T}{\alpha_L} \right) \frac{|\hat{v}_x(\hat{x}, \hat{y})| |\hat{v}_y(\hat{x}, \hat{y})|}{\vec{v}(\hat{x}, \hat{y})} \end{aligned} \tag{B.8}$$

remove eq.

We note that in (B.7) and (B.8), there appear four dimensionless groups:

$$K^* = \frac{K}{N}, \quad \alpha_L^* = \frac{\alpha_L}{L}, \quad \alpha_T^* = \frac{\alpha_T}{\alpha_L} \quad \text{and} \quad D^* = \frac{\eta D_m}{N \alpha_L}. \tag{B.9}$$

In what follows we drop the ‘hat’ notation from the dimensionless formulation.

The objective is to derive an approximate equation for  $C_r(0, y)$ ,  $y < 0$ , and to solve this equation in terms of elementary functions. In the derivation we make use of the fact that the problem with the two drains is symmetric with respect to  $x = 0$ . Hence

$$C_r(x, y) = C_r(-x, y) \quad \text{and thus} \quad \frac{\partial C_r}{\partial x}(0, y) = 0 \quad \text{for any } y < 0. \tag{B.10}$$

The difficulty in finding an equation for  $C_r(0, y)$  is that the coefficient  $d_{xy}(x, y)$  is not differentiable at  $x = 0$ , as sketched in (B.1). Hence we have to avoid taking derivatives in (B.7). Instead, we apply the operator

$$\lim_{\Theta \searrow 0} \frac{1}{2\Theta} \int_{-\Theta}^{\Theta} \dots dx \tag{B.11}$$

to (B.7) for each fixed  $y < 0$ . We do this term by term. In some cases we use the well-known result that, if a function  $f = f(x)$  is continuous near  $x = 0$ , then

$$\lim_{\Theta \searrow 0} \frac{1}{2\Theta} \int_{-\Theta}^{\Theta} f(x) dx = f(0). \tag{B.12}$$

Term 1:

$$\lim_{\Theta \searrow 0} \frac{1}{2\Theta} \int_{-\Theta}^{\Theta} v_x(x, y) \frac{\partial C_r}{\partial x} dx = v_x(0, y) \frac{\partial C_r}{\partial x}(0, y) = 0.$$

Term 2:

$$\lim_{\Theta \searrow 0} \frac{1}{2\Theta} \int_{-\Theta}^{\Theta} v_y(x,y) \frac{\partial C_r}{\partial y} dx = v_y(0,y) \frac{\partial C_r}{\partial y}(0,y).$$

Term 3:

Here we use  $d_{xx}(x,y) = d_{xx}(-x,y)$  and, from (B.10),  $\frac{\partial C_r}{\partial x}(-x,y) = -\frac{\partial C_r}{\partial x}(x,y)$ . Then

$$\begin{aligned} & \frac{1}{2\Theta} \int_{-\Theta}^{\Theta} \frac{\partial}{\partial x} \left( (d_{xx}(x,y) + D^*) \frac{\partial C_r}{\partial x}(x,y) \right) dx = \\ & \frac{1}{2\Theta} \left( (d_{xx}(\Theta,y) + D^*) \frac{\partial C_r}{\partial x}(\Theta,y) - (d_{xx}(-\Theta,y) + D^*) \frac{\partial C_r}{\partial x}(-\Theta,y) \right) = \\ & \frac{1}{2\Theta} (d_{xx}(\Theta,y) + D^*) \left( \frac{\partial C_r}{\partial x}(\Theta,y) - \frac{\partial C_r}{\partial x}(-\Theta,y) \right) \end{aligned}$$

For  $\Theta \searrow 0$ , we have  $(d_{xx}(0,y) + D^*) \frac{\partial^2 C_r}{\partial x^2}(0,y)$ .

Term 4:

Here we use  $d_{xy}(x,y) = d_{xy}(-x,y)$  and, from (B.10),  $\frac{\partial C_r}{\partial y}(-x,y) = -\frac{\partial C_r}{\partial y}(x,y)$ . Then

$$\begin{aligned} & \frac{1}{2\Theta} \int_{-\Theta}^{\Theta} \frac{\partial}{\partial x} \left( d_{xy}(x,y) \frac{\partial C_r}{\partial y}(x,y) \right) dx = \\ & \frac{1}{2\Theta} \left( d_{xy}(\Theta,y) \frac{\partial C_r}{\partial y}(\Theta,y) - d_{xy}(-\Theta,y) \frac{\partial C_r}{\partial y}(-\Theta,y) \right) = 0 \end{aligned}$$

for all  $\Theta > 0$ .

Term 5:

$$\begin{aligned} & \frac{1}{2\Theta} \int_{-\Theta}^{\Theta} \frac{\partial}{\partial y} \left( d_{yx}(x,y) \frac{\partial C_r}{\partial x}(x,y) \right) dx = \\ & \frac{1}{2\Theta} \frac{\partial}{\partial y} \int_{-\Theta}^{\Theta} d_{yx}(x,y) \frac{\partial C_r}{\partial x}(x,y) dx \end{aligned}$$

As  $\Theta \searrow 0$ , there remains

$$\frac{\partial}{\partial y} d_{yx}(0,y) \frac{\partial C_r}{\partial x}(0,y) = 0.$$

Term 6:

$$\begin{aligned} & \lim_{\Theta \searrow 0} \frac{1}{2\Theta} \int_{-\Theta}^{\Theta} \int_{-\Theta}^{\Theta} \frac{\partial}{\partial y} \left( (d_{yy}(x,y) + D^*) \frac{\partial C_r}{\partial y}(x,y) \right) dx = \\ & \frac{\partial}{\partial y} \left( (d_{yy}(0,y) + D^*) \frac{\partial C_r}{\partial y}(0,y) \right) \end{aligned}$$

Combining these results we obtain from (B.7) and operator (B.11)

$$v_y(0,y) \frac{\partial C_r}{\partial y}(0,y) = \frac{\alpha_L}{L} (d_{xx}(0,y) + D^*) \frac{\partial^2 C_r}{\partial x^2}(0,y) + \frac{\alpha_L}{L} \frac{\partial}{\partial y} \left( (d_{yy}(0,y) + D^*) \frac{\partial C_r}{\partial y}(0,y) \right). \tag{B.13}$$

Note that

$$d_{xx}(0, y) = \frac{\alpha_r}{\alpha_l} |v_y(0, y)|$$

and

$$d_{yy}(0, y) = |v_y(0, y)|.$$

Hence,

$$d_{xx}(0, y) = \frac{\alpha_r}{\alpha_l} d_{yy}(0, y). \tag{B.14}$$

Let us now consider the expected contributions of the right hand side terms in (B.13). Based on the numerical simulations in SUTRA, let us, for the sake of the argument, approximate the vertical concentration gradient at  $x = 0$  by a normal Gaussian distribution. The terms  $\frac{\partial C_r}{\partial y}(0, y)$  and  $\frac{\partial^2 C_r}{\partial y^2}(0, y)$  then take the following shape:

$$\frac{\partial C_r}{\partial y}(0, y) \cong \frac{1}{\sigma\sqrt{2\pi}} e^{-\frac{(y-I(0))^2}{2\sigma^2}} \quad \text{and} \quad \frac{\partial^2 C_r}{\partial y^2}(0, y) \cong -\frac{(y-I(0))}{\sigma^3\sqrt{2\pi}} e^{-\frac{(y-I(0))^2}{2\sigma^2}},$$

with  $I(0) = \frac{1}{\pi} \ln\left(\frac{K}{2+K}\right)$  at  $x = 0$  as given in (35). Let us also assume that the vertical concentration at  $x = \Delta x$ , with  $\Delta x$  being a small number, follows the same distribution, with the same standard deviation but a slight upward displacement, with the interface  $I(\Delta x)$  being resolved from (33). We can then approximate the term  $\frac{\partial^2 C_r}{\partial x^2}(0, y)$  numerically, considering that the problem is symmetric with respect to  $x = 0$ .

Assuming a standard deviation  $\sigma = 0.085$ ,  $N = K$  and all other parameters as in the reference simulation, Fig. B.1A shows that this normal Gaussian distribution approximates the mixing zone reasonably well for the given standard deviation.

From Fig. B.1B, we observe that within the mixing zone

$$(d_{xx}(0, y) + D^*) \frac{\partial^2 C_r}{\partial x^2}(0, y) \ll \left| (d_{yy}(0, y) + D^*) \frac{\partial^2 C_r}{\partial y^2}(0, y) \right|,$$

except around the interface position itself, where  $\frac{\partial^2 C_r}{\partial y^2}(0, y) = 0$ . However, we also note that at that position

$$(d_{xx}(0, y) + D^*) \frac{\partial^2 C_r}{\partial x^2}(0, y) \ll -\frac{\partial d_{yy}(0, y)}{\partial y} \frac{\partial C_r}{\partial y}(0, y).$$

Hence, we may argue that the term  $\frac{\alpha_r}{\alpha_l} (d_{xx}(0, y) + D^*) \frac{\partial^2 C_r}{\partial x^2}(0, y)$  can be omitted without large consequences.

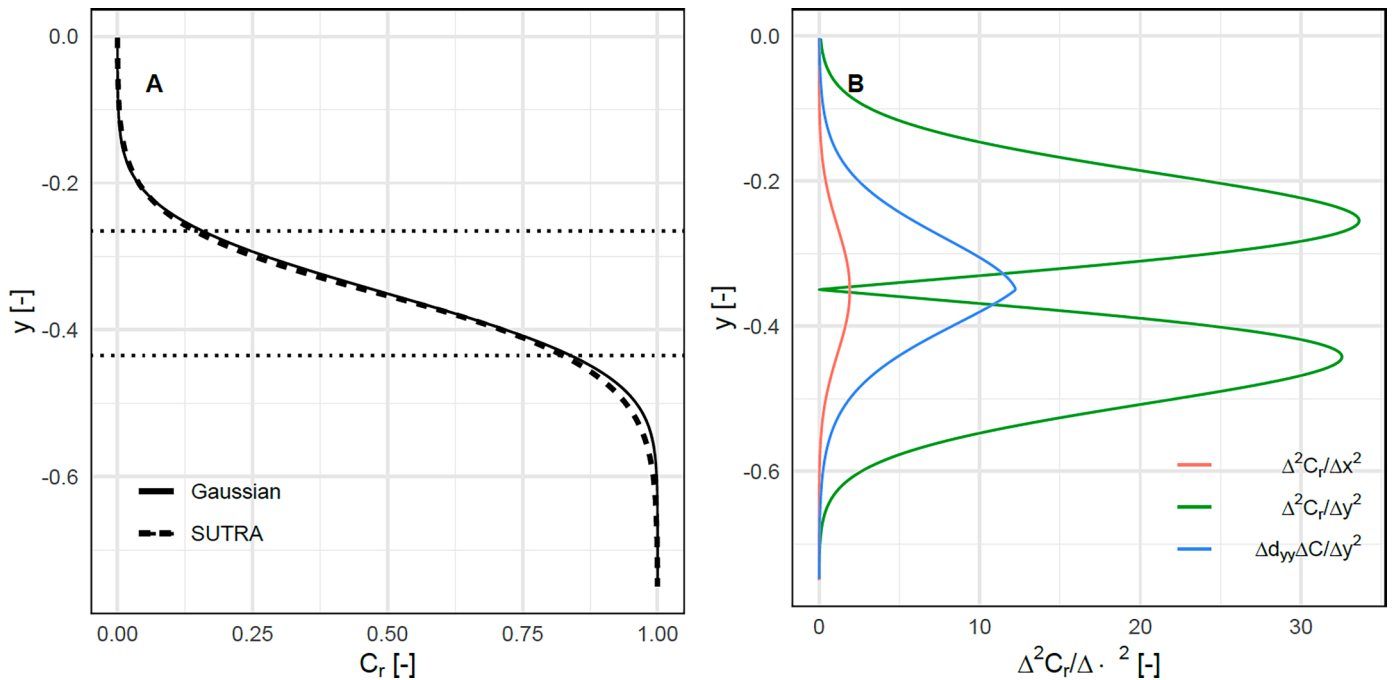


**Fig. B.1.** (A) Vertical concentration profile midway between drains obtained from the reference SUTRA simulation and approximated as a normal Gaussian distribution. Dotted lines indicate interface position plus and minus one standard deviation. (B) Absolute value of the second order derivatives of the concentration with respect to  $y$  midway between the drains for the SUTRA simulation (black dotted) and Gaussian distribution (blue), and second order derivative of the concentration with respect to  $x$  for the Gaussian distribution (red).

What remains is a second order equation for  $C_r(0,y)$  in  $y$ . To simplify the notation we set  $C(y) = C_r(0,y)$  and

$$v(y) = v_y(0,y) = -\left(1 + (1 + K) \frac{e^{\pi y} - 1}{e^{\pi y} + 1}\right). \tag{B.15}$$

The resulting boundary value problem reads

$$\frac{\alpha_L}{L} \frac{d}{dy} \left( (|v(y)| + D^*) \frac{dC}{dy} \right) - v(y) \frac{dC}{dy} = 0 \tag{B.16}$$

for  $-\infty < y < 0$ , subject to

$$C(0) = 0 \text{ and } C(-\infty) = 1. \tag{B.17}$$

To solve (B.16), we introduce the (negative) flux

$$J(y) = (|v(y)| + D^*) \frac{dC}{dy}, \tag{B.18}$$

which satisfies

$$\frac{\alpha_L}{L} \frac{dJ}{dy} - \frac{v(y)}{|v(y)| + D^*} J = 0.$$

Integrating this equation yields

$$J(y) = J(h) e^{-\frac{L}{\alpha_L} \int_h^y \frac{v(\xi)}{|v(\xi)| + D^*} d\xi}. \tag{B.19}$$

Here  $h < 0$  is the location of the interface at  $x = 0$  and  $J(h)$  is the unknown salt flux at that position. Combining (B.18) and (B.19) results in

$$C(y) = 1 + J(h) \int_{-\infty}^y \frac{1}{|v(\xi)| + D^*} e^{-\frac{L}{\alpha_L} \int_h^\xi \frac{v(s)}{|v(s)| + D^*} ds} d\xi. \tag{B.20}$$

This expression satisfies the boundary condition  $C(-\infty) = 1$ . The idea is to choose  $J(h)$  such that  $C(0) = 0$ . To evaluate the integrals in (B.20) we note that

$$|v(y)| = v(y) \text{ if } y < h,$$

$$|v(y)| = -v(y) \text{ if } y > h.$$

We computed (B.20) with the software of Mathematica (Wolfram Research, 2019). The result is as follows:

$$C(y) = 1 + J(h) \operatorname{Re}\{B(y)\} \text{ for } -\infty < y < h, \tag{B.21}$$

with

$$B(y) = B_3 e^{B_1 y} (-K + 2(1 + K) F(b_1, b_2; b_3; b_4(y))) \left( (1 - D^*) \cosh\left(\frac{\pi y}{2}\right) + (1 + K) \sinh\left(\frac{\pi y}{2}\right) \right)^{B_2}. \tag{B.22}$$

Here,  $F(b_1, b_2; b_3; b_4(y))$  is the hypergeometrical function (e.g. Abramowitz and Stegun, 1964). Further,  $B_i$  and  $b_i$  ( $i = 1, 2, 3$ ) are constants and  $b_4(y)$  is a function of  $y$ . They are specified in Table B.1. We take the real part of  $B(y)$  in (B.21) because some of the arguments in  $B(y)$  may be negative.

Similarly, we have

$$C(y) = 1 + J(h) \operatorname{Re}\{A(y) + B(h) - A(h)\} \text{ for } h < y < 0, \tag{B.23}$$

with

$$A(y) = A_3 e^{-A_1 y} (K - 2(1 + K) F(a_1, a_2; a_3; a_4(y))) \left( (1 + D^*) \cosh\left(\frac{\pi y}{2}\right) + (1 + K) \sinh\left(\frac{\pi y}{2}\right) \right)^{A_2}. \tag{B.24}$$

The constants  $A_i$  and  $a_i$  ( $i = 1, 2, 3$ ) and the function  $a_4(y)$  are specified in Table B.1 as well.

Finally, the flux at the interface is obtained from the condition  $C(0) = 0$ :

$$J(h) = -\frac{1}{\operatorname{Re}\{A(0) + B(h) - A(h)\}}. \tag{B.25}$$

**Table B.1**  
Expressions for the dimensionless constants and functions used in (B.22) and (B.24).

Parameter		Expression
$A_1$	=	$\frac{L}{\alpha_L} \frac{(2+K)K - D^*}{(2+K+D^*)(K-D^*)}$
$A_2$	=	$\frac{2L}{\pi \alpha_L} \frac{(1+K)D^*}{(2+K+D^*)(K-D^*)}$
$A_3$	=	$-\frac{1}{(2+K)K} \left(\frac{K}{2+K}\right)^{\frac{A_1}{\pi}} \left(D^* \frac{1+K}{K} \sqrt{\frac{K}{2+K}}\right)^{-A_2}$
$a_1$	=	1
$a_2$	=	$-\frac{1}{\pi} \frac{L}{\alpha_L} \frac{2+K}{2+K+D^*}$
$a_3$	=	$1 - \frac{1}{\pi} \frac{L}{\alpha_L} \frac{K}{K-D^*}$
$a_4$	=	$\frac{2+K+D^*}{K-D^*} e^{\pi y}$
$B_1$	=	$\frac{L}{\alpha_L} \frac{(2+K)K + D^*}{(2+K-D^*)(K+D^*)}$
$B_2$	=	$\frac{2L}{\pi \alpha_L} \frac{(1+K)D^*}{(2+K-D^*)(K+D^*)}$
$B_3$	=	$\frac{1}{(2+K)K} \left(\frac{K}{2+K}\right)^{\frac{B_1}{\pi}} \left(-D^* \frac{1+K}{K} \sqrt{\frac{K}{2+K}}\right)^{-B_2}$
$b_1$	=	1
$b_2$	=	$\frac{1}{\pi} \frac{L}{\alpha_L} \frac{2+K}{2+K+D^*}$
$b_3$	=	$1 + \frac{1}{\pi} \frac{L}{\alpha_L} \frac{K}{K+D^*}$
$b_4(y)$	=	$\frac{2+K+D^*}{K+D^*} e^{\pi y}$

## References

- Abramowitz, M., Stegun, I.A., 1964. Handbook of mathematical functions with formulas, graphs, and mathematical tables. Appl. Math. Ser. Vol. 55. Washington D.C. ISBN 978-0-486-61272-0.
- Alt, H.W., van Duijn, C.J., 1990. A stationary flow of fresh and salt groundwater in a coastal aquifer. Nonlin. Anal. Theor. Methods Appl. 14, 625–656. [https://doi.org/10.1016/0362-546X\(90\)90042-F](https://doi.org/10.1016/0362-546X(90)90042-F).
- Badon Ghijben, W., 1888. Nota in verband met de voorgenomen putboring nabij Amsterdam [Note on the planned well drilling near Amsterdam]. *Tijdschrift van het Koninklijk Instituut van Ingenieurs, Den Haag*. 1888/9, pp. 8–22.
- Bedford, B.L., Godwin, K.S., 2003. Fens of the United States: Distribution, characteristics, and scientific connection versus legal isolation. *Wetlands* 23, 608–629. [https://doi.org/10.1672/0277-5212\(2003\)023\[0608:FOTUSD\]2.0.CO;2](https://doi.org/10.1672/0277-5212(2003)023[0608:FOTUSD]2.0.CO;2).
- Carol, E., Richiano, S., Tanjal, C., 2018. Can bioturbation be responsible for thicker freshwater lenses than expected in littoral environments? *Mar. Freshwater Res.* 69 (4), 542–550. <https://doi.org/10.1071/MF17253>.
- Chan Hong, J.R., van Duijn, C.J., Hilhorst, D., van Kester, J., 1989. The interface between fresh and salt groundwater: a numerical study. *IMA J. Appl. Math.* 42, 209–240. <https://doi.org/10.1093/imamat/42.3.209>.
- Cirkel, D.G., van Beek, C.G.E.M., Witte, J.P.M., van der Zee, S.E.A.T.M., 2014. Sulphate reduction and calcite precipitation in relation to internal eutrophication of groundwater fed alkaline fens. *Biogeochemistry*. 117, 375–393. <https://doi.org/10.1007/s10533-013-9879-4>.
- Cirkel, D.G., van der Zee, S.E.A.T.M., Meeussen, J.C.L., 2015. Front spreading with nonlinear sorption for oscillating flow. *Water Resour. Res.* 51, 2986–2993. <https://doi.org/10.1002/2014WR015847>.
- Cozzolino, D., Greggio, N., Antonellini, M., Giambastiani, B.M.S., 2017. Natural and anthropogenic factors affecting freshwater lenses in coastal dunes of the Adriatic coast. *J. Hydrol.* 551, 804–818. <https://doi.org/10.1016/j.jhydrol.2017.04.039>.
- van de Craats, D., van der Zee, S.E.A.T.M., Leijnse, A., 2021. Anticipatory drainage base management for groundwater level optimization. *Water Resour. Res.* 57, e2021WR029623 <https://doi.org/10.1029/2021WR029623>.
- van de Craats, D., van Duijn, C.J., Raats, P.A.C., 2024. Interface and mixing zone between soil water arising from upward and downward seepage – Part II: heterogeneous total density. In: *Adv. Water. Resour.* <https://doi.org/10.1016/j.advwatres.2024.104794>, 104794.
- Delsman, J.R., de Louw, P.G.B., de Lange, W.J., Oude Essink, G.H.P., 2017. Fast calculation of groundwater exfiltration salinity in a lowland catchment using a lumped celerity/velocity approach. *Environ. Modell. Software* 96, 323–334. <https://doi.org/10.1016/j.envsoft.2017.07.004>.
- van Duijn, C.J., van der Zee, S.E.A.T.M., 1986. Solute transport parallel to an interface separating two different porous materials. *Water Resour. Res.* 22, 1779–1789. <https://doi.org/10.1029/WR022013p01779>.
- van Duijn, C.J., van der Zee, S.E.A.T.M., 2018. Large time behaviour of oscillatory nonlinear solute transport in porous media. *Chem. Eng. Sci.* 183, 86–94. <https://doi.org/10.1016/j.ces.2018.02.045>.
- Eeman, S., Leijnse, A., Raats, P.A.C., van der Zee, S.E.A.T.M., 2011. Analysis of the thickness of a fresh water lens and of the transition zone between this lens and upwelling saline water. *Adv. Water. Resour.* 34, 291–302. <https://doi.org/10.1016/j.advwatres.2010.12.001>.
- Eeman, S., van der Zee, S.E.A.T.M., Leijnse, A., de Louw, P.G.B., Maas, C., 2012. Response to recharge variation of thin rainwater lenses and their mixing zone with underlying saline groundwater. *Hydrol. Earth Syst. Sci.* 16, 3535–3549. <https://doi.org/10.5194/hess-16-3535-2012>.
- Groenendijk, P., van den Eertwegh, G.A.P.H., 2004. Drainage-water travel times as key factor for surface water contamination. In: Feddes, R.A., de Rooij, G.H., van Dam, J. C. (Eds.), *Unsaturated-zone modelling: progress, challenges and applications* (145–178). Wageningen UR Frontis Series (6).
- Herbert, E.R., Boon, P., Burgin, A.J., Neubauer, S.C., Franklin, R.B., Ardón, M., Hopfensperger, K.N., Lamers, L.P.M., Gell, P., 2015. A global perspective on wetland salinization: ecological consequences of a growing threat to freshwater wetlands. *Ecosphere* 6 (10), 206. <https://doi.org/10.1890/ES14-00534.1>.
- Herzberg, A., 1901. Die Wasserversorgung einiger Nordseebäder. [The water supply of some North Sea spas]. *J. Gasbeleucht. Wasserversorg.* 44, 842–844, 815–819; 45.
- de Josselin de Jong, G., 1960. Singularity distributions for the analysis of multiple-fluid flow through porous media. *J. Geophys. Res.* 65, 3739–3758. <https://doi.org/10.1029/JZ065i011p03739>.
- de Louw, P.G.B., Eeman, S., Siemon, B., Voortman, B.R., Gunnink, J., van Baaren, E.S., Oude Essink, G.H.P., 2011. Shallow rainwater lenses in deltaic areas with saline seepage. *Hydrol. Earth Syst. Sci.* 15, 3659–3678. <https://doi.org/10.5194/hess-15-3659-2011>.
- de Louw, P.G.B., Eeman, S., Oude Essink, G.H.P., Vermue, E., Post, V.E.A., 2013. Rainwater lens dynamics and mixing between infiltrating rainwater and upward saline groundwater seepage beneath a tile-drained agricultural field. *J. Hydrol.* 501, 133–145. <https://doi.org/10.1016/j.jhydrol.2013.07.026>.
- Maas, K., 2007. Influence of climate change on a Ghijben–Herzberg lens. *J. Hydrol.* 347, 223–228. <https://doi.org/10.1016/j.jhydrol.2007.09.020>.
- Marconi, V., Antonellini, M., Balugani, E., Dinelli, E., 2011. Hydrogeochemical characterization of small coastal wetlands and forests in the Southern Po plain (Northern Italy). *Ecohydrol* 4, 597–607. <https://doi.org/10.1002/eco.204>.
- Pauw, P.S., 2015. *Field and Model Investigations of Freshwater Lenses in Coastal Aquifers*, 159 pages. PhD thesis. Wageningen University, Wageningen, the Netherlands. ISBN 978-94-6257-292-8.
- Pauw, P.S., van Baaren, E.S., Visser, M., de Louw, P.G.B., Oude Essink, G.H.P., 2015. Increasing a freshwater lens below a creek ridge using a controlled artificial recharge and drainage system: a case study in the Netherlands. *Hydrogeol. J.* 23, 1415–1430. <https://doi.org/10.1007/s10040-015-1264-z>.
- Poot, A., Schot, P.P., 2000. Regenwaterlenzen: vorm en dynamiek (Rainwater lenses: form and dynamics). *Stromingen* 6, 13–26.
- Schot, P.P., Dekker, S.C., Poot, A., 2004. The dynamic form of rainwater lenses in drained fens. *J. Hydrol.* 293, 74–84. <https://doi.org/10.1016/j.jhydrol.2004.01.009>.

- Stofberg, S.F., van Engelen, J., Witte, J.P.M., van der Zee, S.E.A.T.M., 2016. Effects of root mat buoyancy and heterogeneity on floating fen hydrology. *Ecohydrol* 9, 1222–1234. <https://doi.org/10.1002/eco.1720>.
- Stofberg, S.F., Oude Essink, G.H.P., Pauw, P.S., de Louw, P.G.B., Leijnse, A., van der Zee, S.E.A.T.M., 2017. Fresh water lens persistence and root zone salinization hazard under temperate climate. *Water Resour. Manage.* 31, 689–702. <https://doi.org/10.1007/s11269-016-1315-9>.
- Vandenbohede, A., Mollema, P.N., Greggio, N., Antonellini, M., 2014. Seasonal dynamic of a shallow freshwater lens due to irrigation in the coastal plain of Ravenna, Italy. *Hydrogeol. J.* 22, 893–909. <https://doi.org/10.1007/s10040-014-1099-z>.
- Velstra, J., Groen, J., de Jong, K., 2011. Observations of salinity patterns in shallow groundwater and drainage water from agricultural land in the northern part of the Netherlands. *Irrig. Drain.* 60, 51–58. <https://doi.org/10.1002/ird.675>.
- Voss, C.I., Provost, A.M., 2002. SUTRA, a model for saturated-unsaturated variable-density groundwater flow with solute or energy transport (version september 22, 2010). Report 02-4231, 291 pages. US Geological Survey. [Water Resources Investigations](https://doi.org/10.1002/eco.1720).
- Wassen, M.J., Joosten, J.H.J., 1996. In search of a hydrological explanation for vegetation changes along a fen gradient in the Biebrza Upper Basin (Poland). *Vegetatio* 124 (2), 191–209. <https://doi.org/10.1007/BF00045494>.
- Werner, A.D., Bakker, M., Post, V.E.A., Vandenbohede, A., Lu, C., Ataie-Ashtiani, B., Simmons, C.T., Barry, D.A., 2013. Seawater intrusion processes, investigation and management: Recent advances and future challenges. *Adv. Water Resour.* 51, 3–26. <https://doi.org/10.1016/j.advwatres.2012.03.004>.
- Wolfram Research (2019). *Mathematica Version 12.0*. Champaign, IL, US.
- van der Zee, S.E.A.T.M., 1988. *Transport of reactive contaminants in heterogeneous soil systems*. 283 pages. PhD thesis. Wageningen University, Wageningen, the Netherlands.